

RIZOMILOS2

Archaeological Background

Rizomilos 2 magoula is a low but extensive hill made by the continuous habitation throughout the Neolithic Period and until the Early Bronze Age. Apart from the finds on the magoula there are several potsherds and other minor prehistoric objects (like stone tools) scattered over a large area in the northeast of the site just beyond the magoula itself. Being one of the oldest Neolithic settlements of the area, it appears as a settlement which endured for several millennia too. From that point of view it is a very interesting and promising archaeological site.

Satellite Remote Sensing and Historical Aerial Photography Survey

A GeoEye-1 image from 4 May 2010 (Figure 1) and a Quickbird image from 7 January 2004 (Figure 2) were used for satellite remote sensing at Rizomilos 2. The GeoEye-1 has an off-nadir angle of 9.9° and a ground sampling distance (GSD) of 0.50 m (panchromatic) and 1.81 m (multispectral). The Quickbird has an off-nadir angle of 29.4° and a GSD of 0.77 m (panchromatic) and 3.09 m (multispectral). In addition to the satellite imagery, two aerial photographs from 26 August 1960 with a scale of 1:15,000 and 19 May 1982 with a scale of 1:30,000 were used in the analysis (Figure 3).

The landscape around Rizomilos 2 is level agricultural terrain that rises gradually toward the west beyond the National Road (2.5 km away). Various streams and irrigation channels pocket the terrain. There are few modern constructions apart from a scattering of farm installations. The modern village of Rizomilos is a little more than 1 km southeast of the prehistoric tell. Cultivation in the region is predominantly wheat and other low standing vegetation. There are no olive and citrus orchards. Elevations range from 60-70 masl around the target site.

The local environment and land use around Rizomilos 2 have not undergone significant changes. Some field boundaries and field orientations are different in the 23 August 1960 aerial photograph than they appear in the 4 May 2010 GeoEye-1. However, one substantial change is the construction of a large poultry farm on the summit of the prehistoric mound and a small house to the southeast. These installations were not present in the 2004 Quickbird, but they are in the 2010 GeoEye-1.

Satellite remote sensing within a 1 km radius around Rizomilos 2 produced excellent results (Figures 4-5). Many features correspond to palaeochannels (blue) associated with the rivers and streams that once pocketed the terrain. Some other anomalies relate to agricultural activity (brown), such as former field divisions and plow lines. A third category of anomalies is unclassified (yellow). There are enough surface anomalies and localized vegetation stress to betray the presence of a sizable settlement of ovalar form, approximately 450 m x 250 m. The clarity in which the dimensions and boundaries of the prehistoric tell appear in the satellite imagery is unusual compared to other prehistoric mounds in the region. A true color RGB and various feature enhancement indices from the 2010 GeoEye-1 show the settlement in good detail; however, the 2004 Quickbird image displays an amazing amount of detail in true color RGB and feature enhancement indices (Figure 6). The data from satellite remote sensing goes a

long way in defining the size of Rizomilos 2, showing that habitation activity extended well beyond the top of the prehistoric mound.

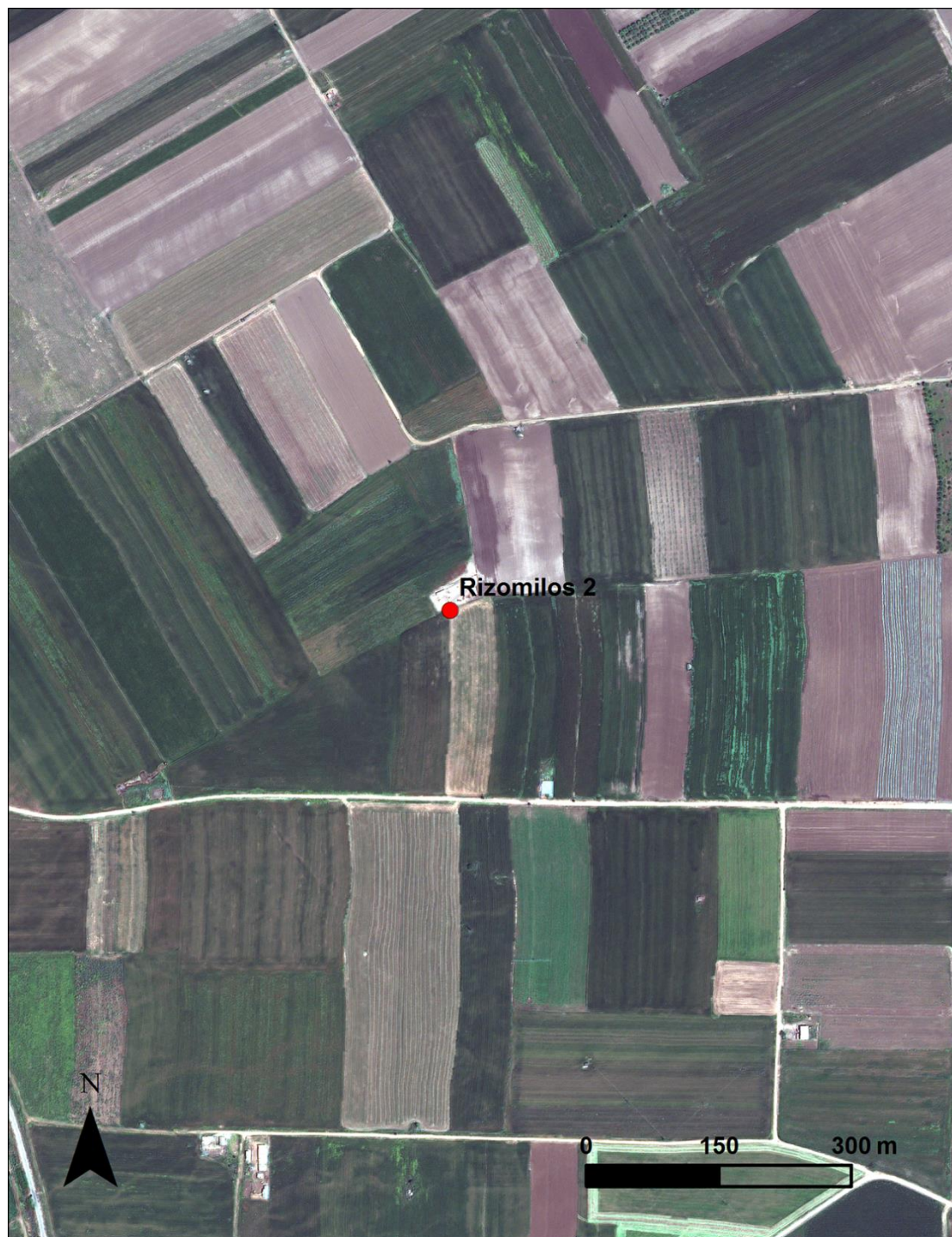


Figure 1: Rizomilos 2 from a 4 May 2010 GeoEye-1 image



Figure 2: Rizomilos 2 from a 7 January 2004 Quickbird image



Figure 3: Rizomilos 2 from aerial photographs taken 26 August 1960 (left) and 19 May 1982 (right)

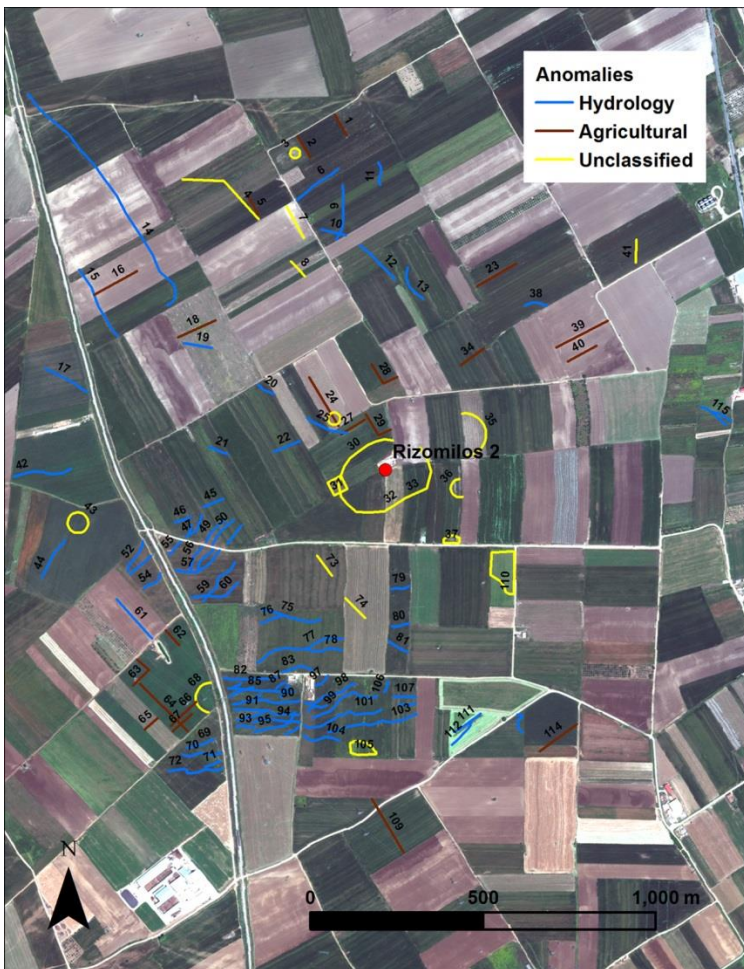


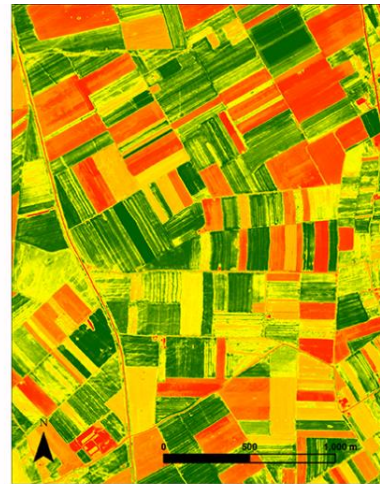
Figure 4: Surface anomalies from the 4 May 2010 GeoEye-1 image within a 1 km radius around Rizomilos 2



PCA



ARVI



Green NDVI



MSAVI



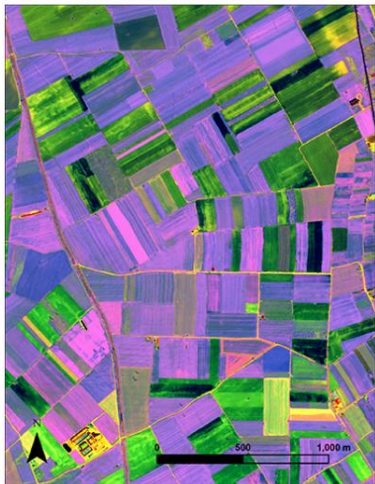
MSR



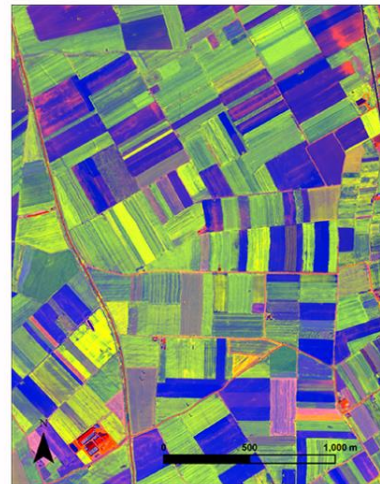
NDVI



Decorrelation Stretch



RGB to IHS



Tasseled Cap

Figure 5: Spectral filters and vegetation indices applied to the 4 May 2010 GeoEye-1 image around Rizomilos 2

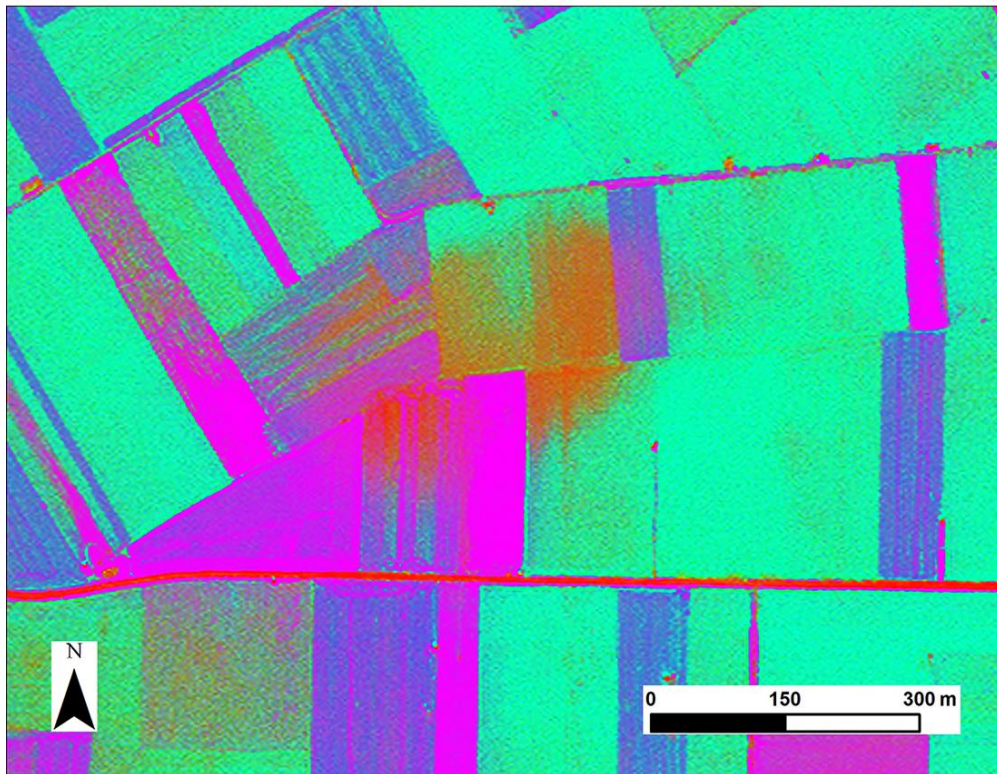
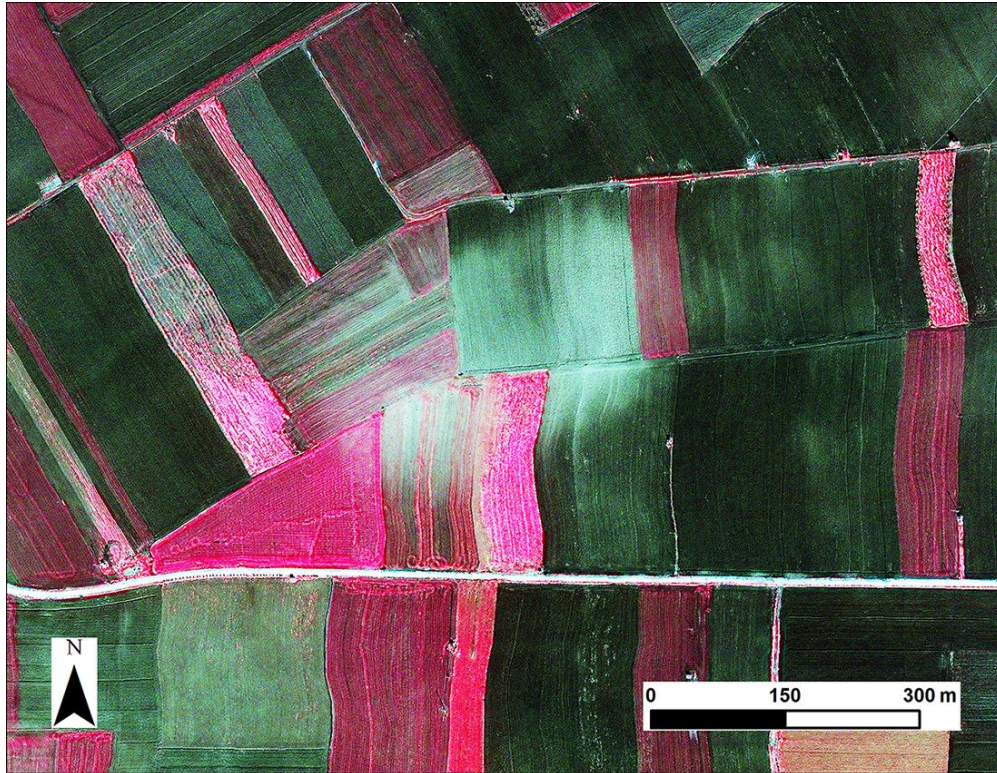


Figure 6: Globular anomaly related to the prehistoric settlement of Rizomilos 2 from the 7 January 2004 Quickbird. Top: infrared 4-3-2 band ratio. Bottom: Tasseled Cap

Remotely Piloted Aircraft Systems (RPAS) Survey

The site of Rizomilos2 has been photographed with all available cameras (GoPro, regular RGB and modified NIR), but no relevant trace could be identified during their analysis. Also the DEMs produced in photogrammetry didn't return any particular altimetric anomaly of interest. The examination of the internet orthophotos instead gave some additional information to integrate with the results from geophysics.

In particular, a white halo in correspondence with the main centroid of the magoula can be seen in almost all images, the ones accessible through Google and Bing and the National orthophoto from the Ktimatologio. The most interesting of them seems to be the last one, where the edges of the halo is more defined and seems to suggest an elongated shape for the magoula, possibly related with a multi core organization or successive occupation dislocation.



Figure 7: Orthophoto from the Ktimatologio (preceding the construction of the storage-house/farm approximately in the center of the frame) with the results from geophysics in overlay. Note the North-Eastern side of the magoula (red arrows), where the halo seems to extend further.

Geophysical Prospection Geomagnetic Survey

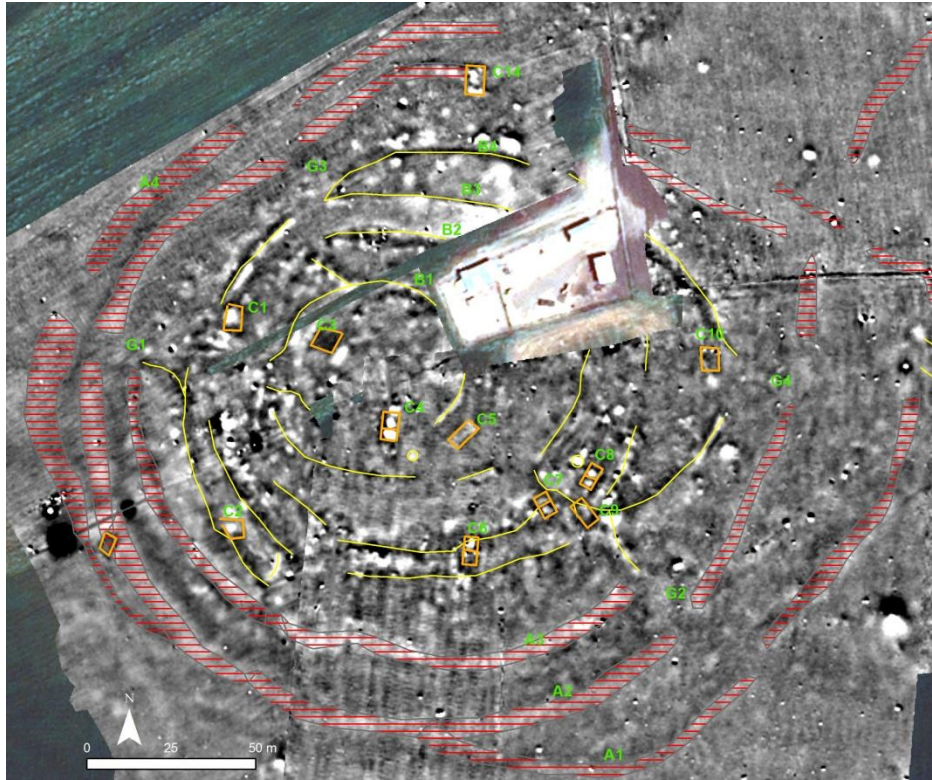


Figure 8: Geomagnetic results from the core of the settlement

Rizomilos2 geomagnetic data immediately reveals a concentric shape for the magoula. This is visible through circular anomalies enveloping the magoula (A1, A2, A3, and A4). While the inner zone is the most circular, outer enclosures are relatively more deformed in shape. These anomalies do not possess continuous geomagnetic readings, but have breaks at specific locations. These breaks might be representing the openings (“the doors”) to the magoula (G1, G2, G3, and G4). Despite the high definition of ditches, no architectural anomalies are apparent in between enclosures. In fact, the distance between these anomalies are not wide enough to host habitation. Thus, it raises the possibility that these features were built for defensive purposes and indirectly for supplying building material for the daub structures.

Geomagnetic data gets more heterogeneous to the center of the magoula —albeit without a clear indication for spatial patterning. The evidence for built environment is scattered at best and no anomaly clearly represents itself as an architectural feature.

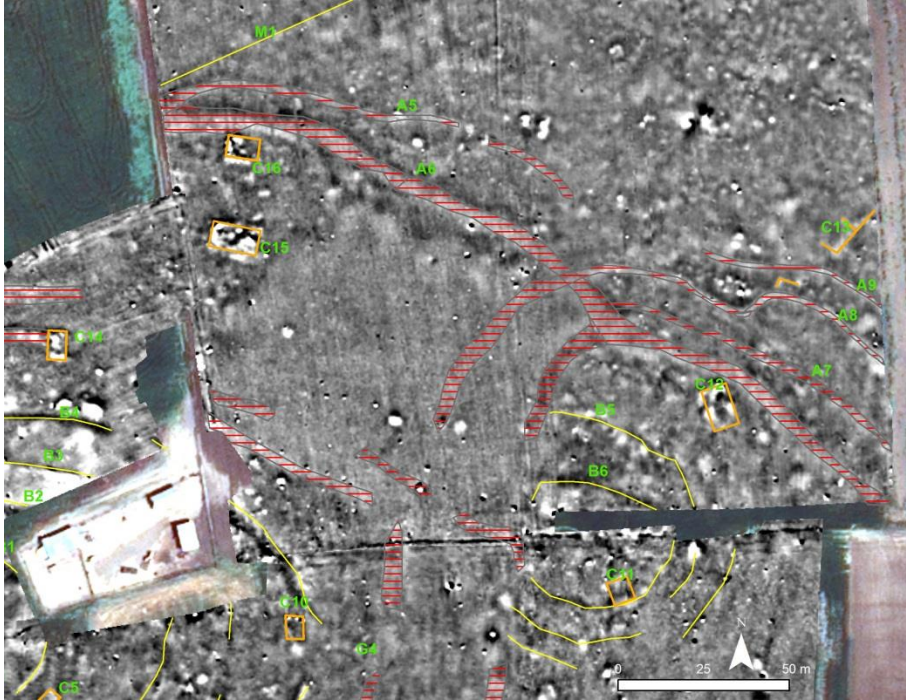


Figure 9: The secondary settlement core to the east of the main settlement

Yet another settlement core is located to the east of the main tell. This settlement is also circular in shape and surrounded by a series of enclosures (A7 and A8). The long linear anomaly A6 may be of natural origins —due to its shape and location with respect to each settlement. Without proper archaeological excavations we cannot immediately talk about contemporaneity of these settlements. However, considering the spatial configuration of enclosures, these settlements appear as belonging to different time periods. Due to the truncation of the enclosures in the west, it seems that this settlement predates the main magoula. Like in the main tell, inner enclosures (B5 and B6) further delineate the settlement. Due to the background, it is not possible to discern any “gates” in this settlement, if they ever existed.

There is no discernable architecture in this smaller settlement, other than a potential feature C12 which is located outside of the inner enclosures (B5 & B6). Therefore, it is not possible to have a comparison between these two neighboring settlements other than their apparently similar shapes and the configurations of enclosures.

Electromagnetic Induction Survey

EM survey was done with the GEM2 from Geophex and with the CMD mini-explorer from GF Instruments with a GPS positioning. The use of both of these instruments presents the advantage to give valuable information for two depths of investigation and three geophysical parameters (magnetic susceptibility at 1.6 m for the GEM2 and 1.3 m for the CMD min-explorer). Both instruments were not used to cover the same area. The GEM2 was implemented at the core site and the CMD on the north part of the site. For the CMD, three depths of investigation for electrical conductivity and two depths of investigation for magnetic susceptibility are presented below.

Generally speaking, results are poor in term of archaeological evidence. Contrast of magnetic susceptibility is not good enough to overpass the global noise of this area. On the north part of the site the susceptibility is very noisy. This comes from the HCP configuration which is not well adapted for this parameter. However the HCP geometries were used as they are the best geometries for the electrical conductivity mapping. For the GEM2 the problem is different. As this instrument uses a bucking coil, the characteristic of the HCP geometry changes completely. In this case HCP measurement is suitable for the magnetic susceptibility as well as for the electrical conductivity.

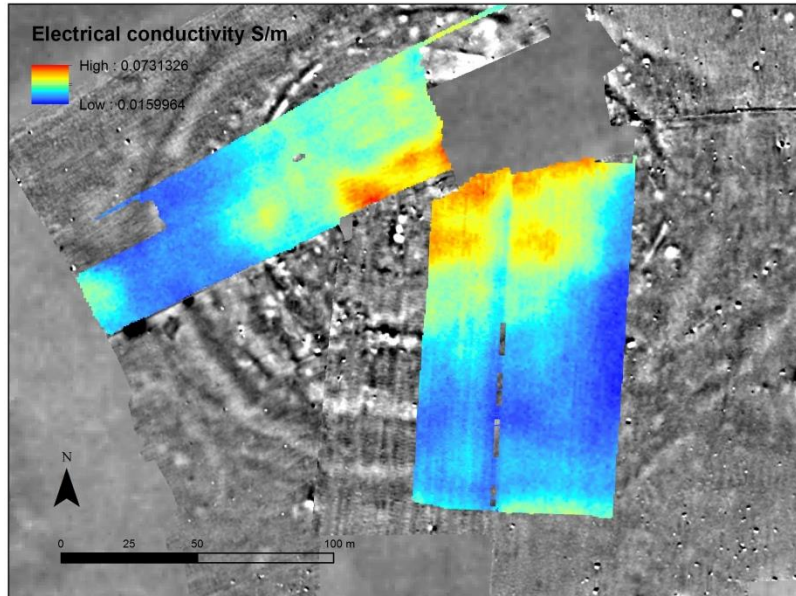


Figure 10: Apparent electrical conductivity (GEM2 – HCP – Depth of investigation : 0-2.5 meter)

For a large depth of investigation (in relation with our target) the electrical conductivity shows a global distribution close to our knowledge for this site. On the top of the magoula, the conductivity is higher than on the slope. We observe four different levels of electrical conductivity. The first one is located on the extremity, after the anomaly corresponding to a ditch. This corresponds probably with the global value of the electrical conductivity in the natural context. On the top of the magoula a very high conductivity delimits the central part of the magoula. A second level less conductive is demilited by the C1 anomalies. This level of conductivity probably demilits the extension of the inhabited area. After one, the value of conductivity are very low corresponding to the ditches area. This difference could come from the nature of the sediment as the settled part contains higher clay content. On the VCP we observe the same general variation with a level of noise slightly higher. This indicates the existence of this difference on the top part of the soil.

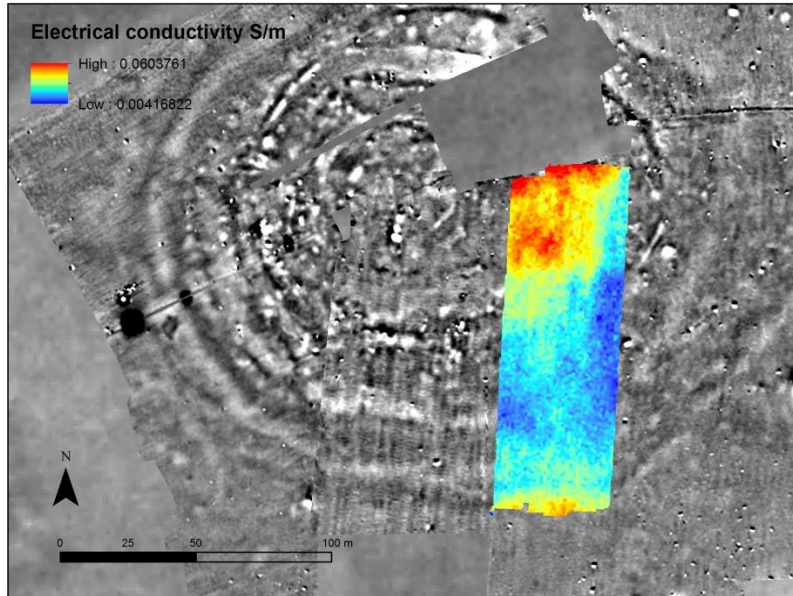


Figure 11: Apparent electrical conductivity (GEM2 – VCP – Depth of investigation : 0-1.6 meter)

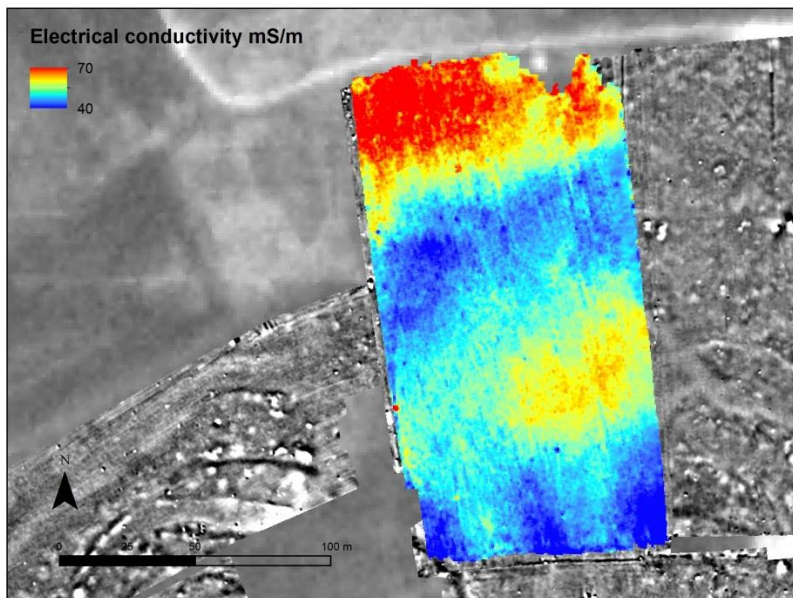


Figure 12: Apparent electrical conductivity (CMD – HCP – depth of investigation : 0-0.5 meter)

On the north part of the site, the electrical conductivity shows some variations mainly related to the flood deposit in this area. On the north part the conductivity is very high where in between this area and the settlement the value of electrical conductivity are lower (as for the GEM2 on the main part of the settlement). We can conclude that this area contains a gravel/sandy deposit on top of the flood deposit in contrast to the fine clay sediment of the settlement.

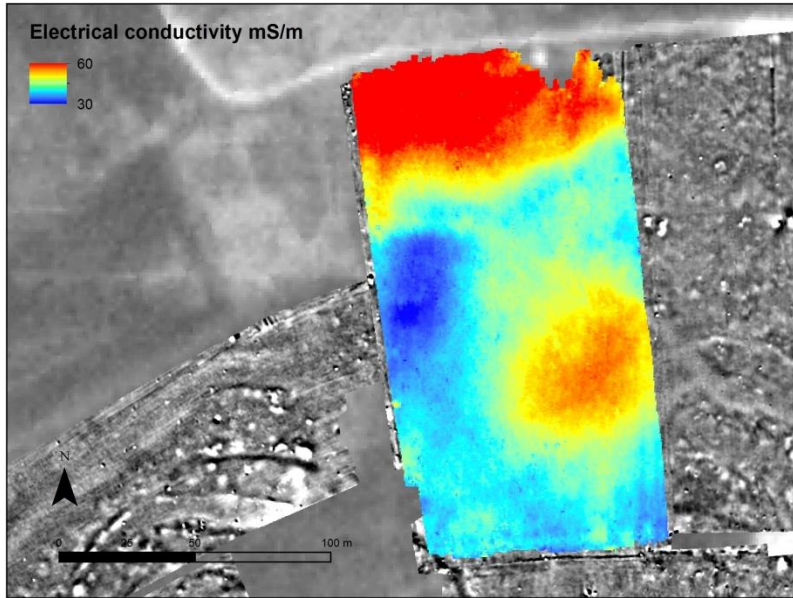


Figure 13: Apparent electrical conductivity (CMD – HCP – depth of investigation : 0-1 meter)
 At 1 meter depth, the noise is lower as the measurement includes a larger volume of soil.

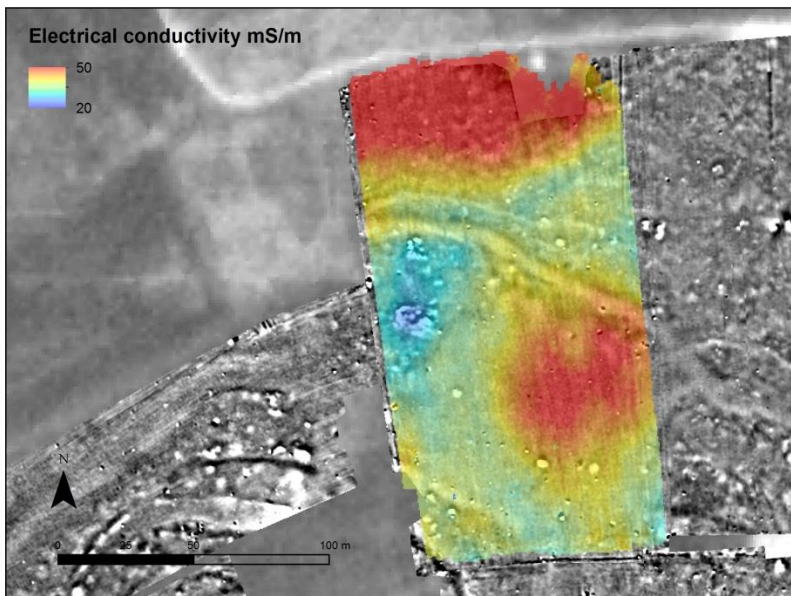


Figure 14: Apparent electrical conductivity (CMD – HCP – Depth of investigation : 0-1.8 meter)

We present here (Figure 14) the value of the electrical conductivity superimposed on the magnetic result. We observe that the linear magnetic anomalies follow the same direction given by the electrical conductivity in the blue area. On the last figure we observe the evidence of a building disconnected to the main settlement. This one seems connected to the blue area (as the main part of the linear anomalies).

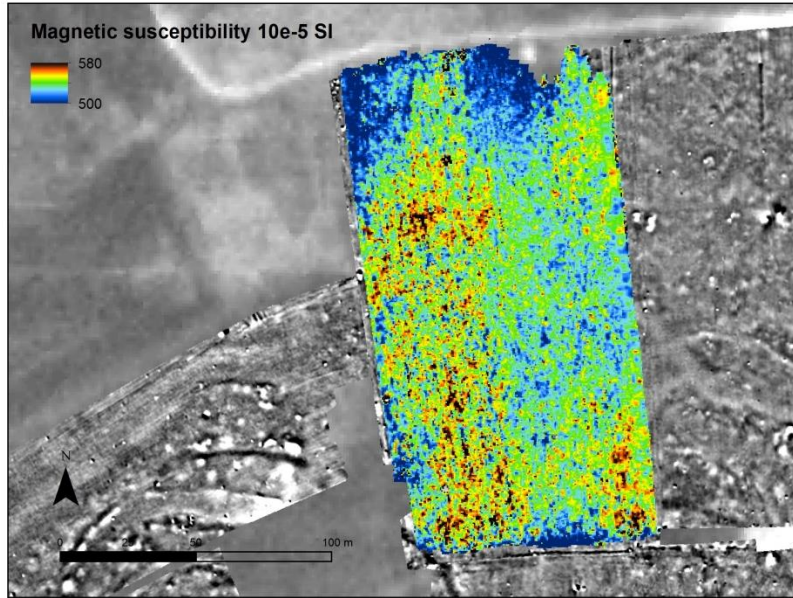


Figure 15: Apparent magnetic susceptibility (CMD – HCP – Depth of investigation : 0-0.7 meter)

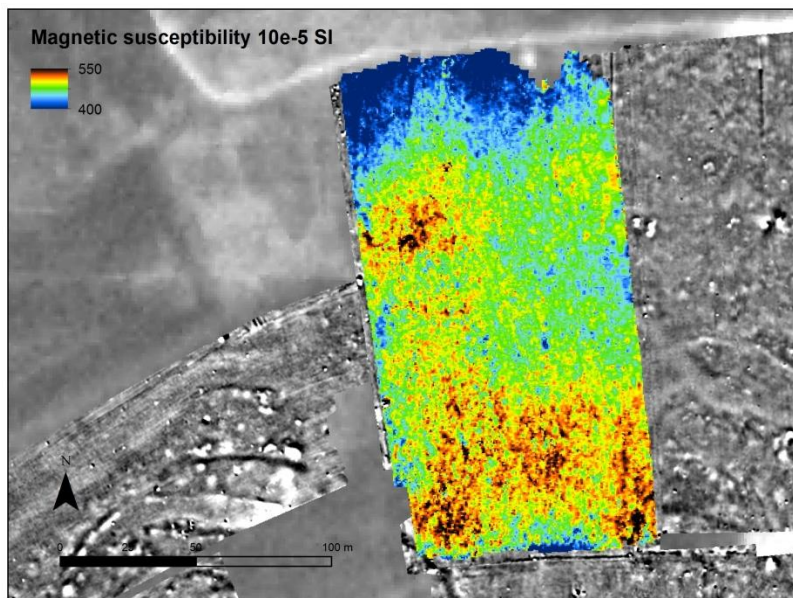


Figure 16: Apparent magnetic susceptibility (CMD – HCP – Depth of investigation : 0-1.3 meter)

On the north part the magnetic susceptibility doesn't show clear information about archaeological evidence as this parameter is very noisy. Nevertheless we observe a decrease of the magnetic susceptibility with the north (which is related to the distance with the core settlement). The map doesn't show any archaeological evidence.

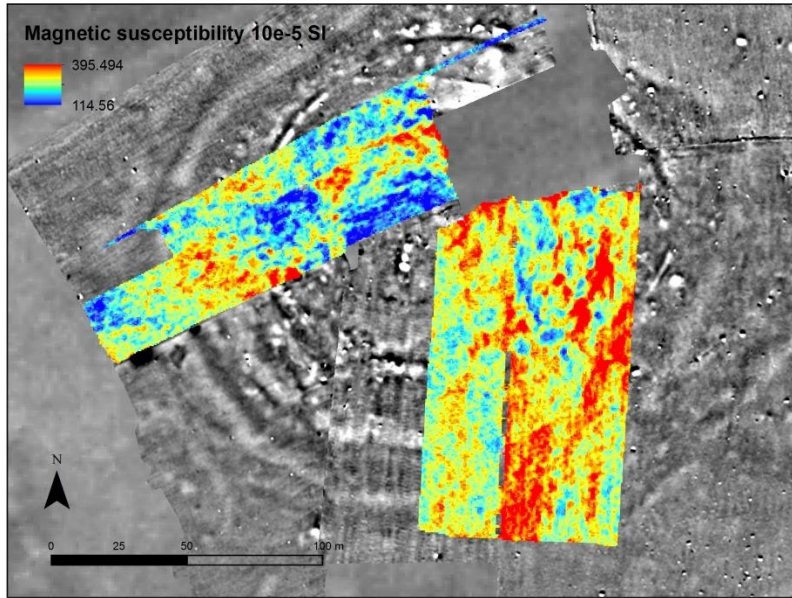


Figure 17: Apparent magnetic susceptibility (CMD – HCP – Depth of investigation : 0-1.6 meter)

On the central part of the site, the magnetic susceptibility is more valuable even if the map presents a high level of noise (partially removed by different spatial filtering). Many anomalies observed on the magnetic map are present (C3, C8, B2, etc.). The ditches are not visible on this map. Different hypotheses could explain this lack of anomalies: a low magnetic contrast between the filling and the background or a geometry which is not compatible with the EM detection capability. The value of this map concerns essentially the depth of investigation of the recognized anomalies as the magnetic measurement doesn't allow an accurate depth estimation.

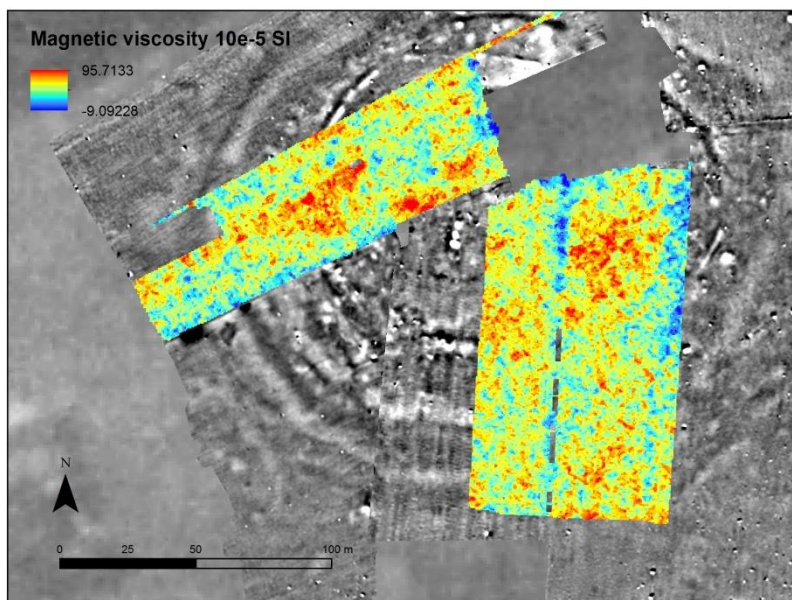


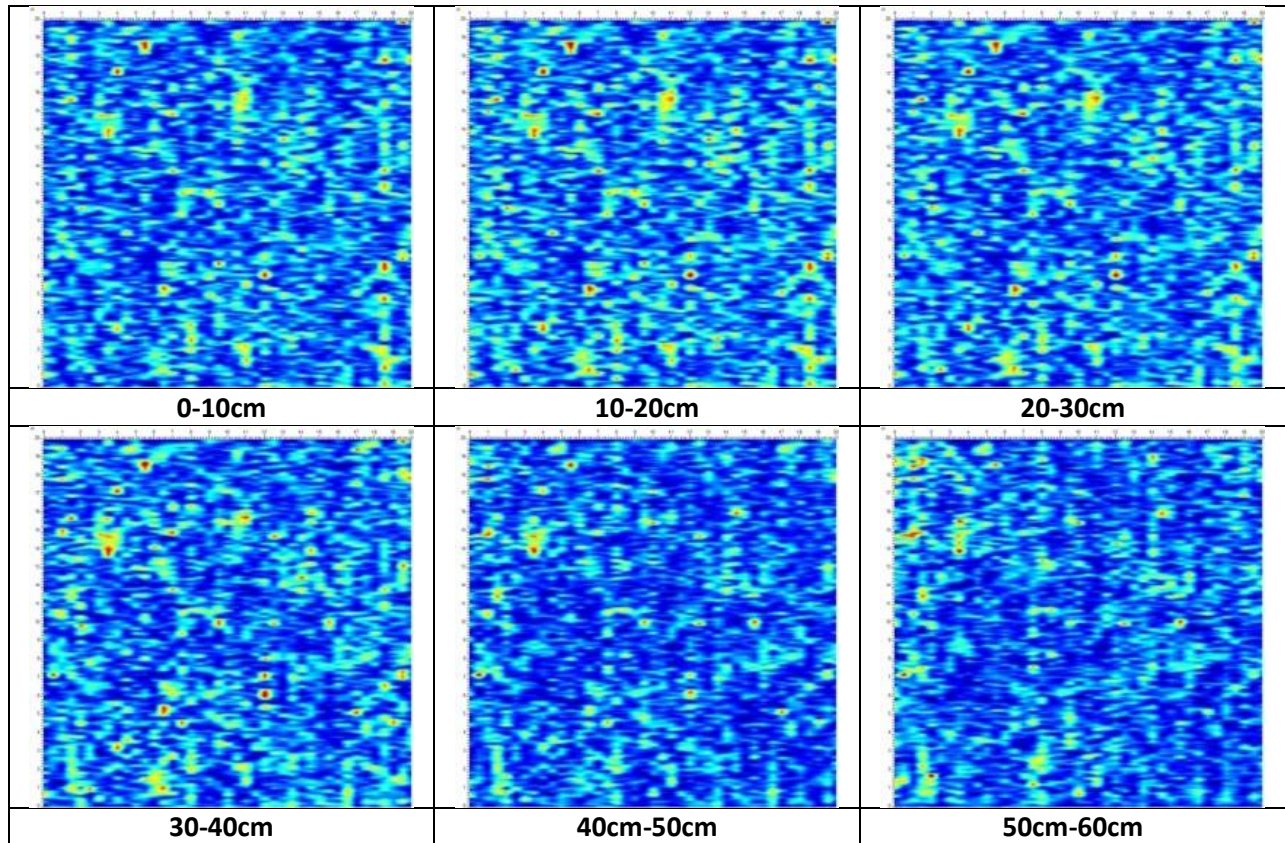
Figure 18: Apparent magnetic viscosity (GEM2 – HCP – Depth of investigation : 0-1.6 meter)

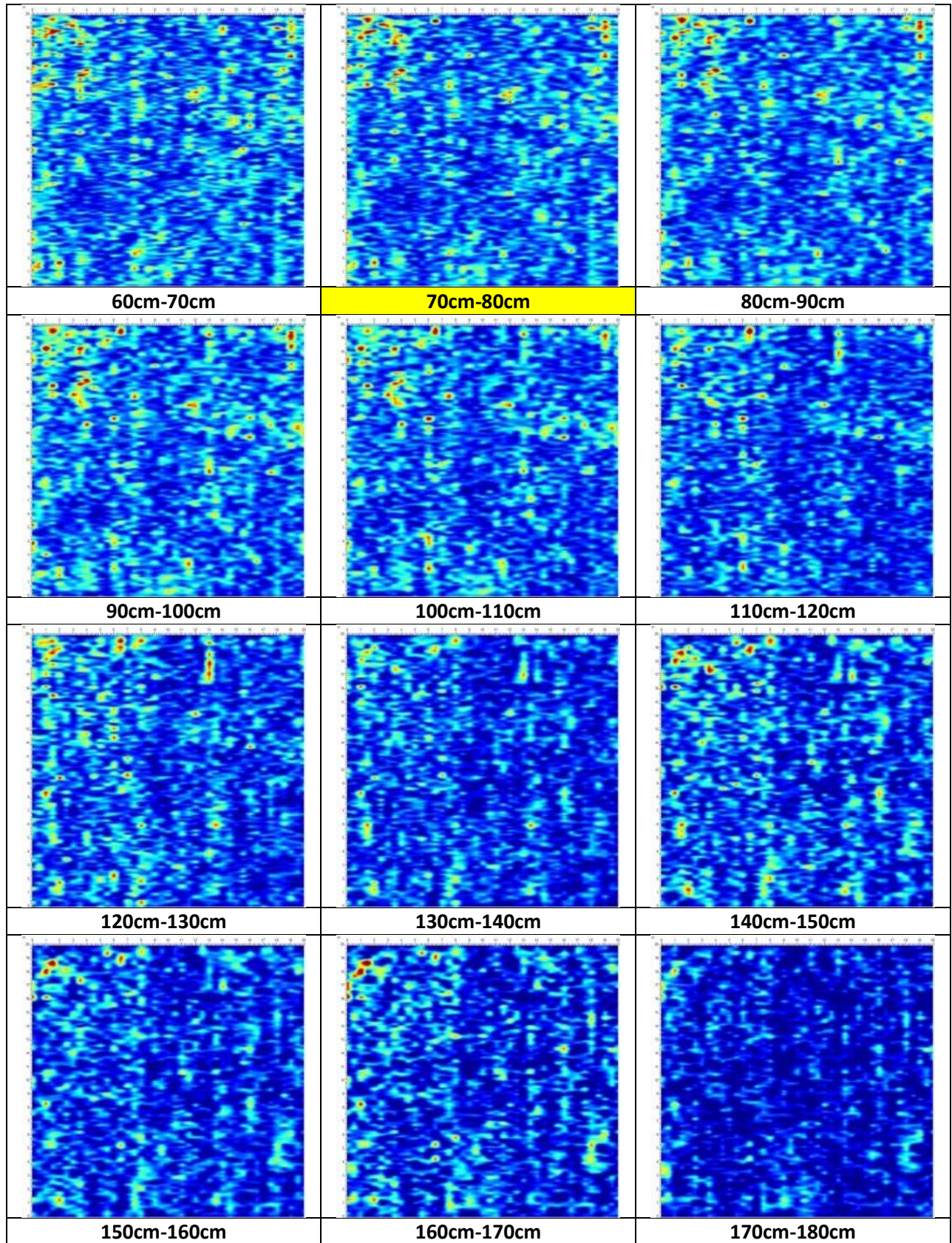
The magnetic viscosity is clearly correlated with the magnetic susceptibility. On the top part of the site we observe some anomalies presenting a high value of viscosity. They could correspond to a fire place or burned material. In terms of location, this parameter seems more suitable than the magnetic susceptibility for the recognition of features with high magnetic properties. It is interesting then to focalize on C2 and C10, which correspond to small buildings and are connected with a layer of magnetic material. These two places are then probably linked with specific activities on this settlement.

Ground Penetrating Radar Survey

GRID: RIZOMILOS1

Trace reposition, Repick first break (25%), Dewow, SEC2 (Atn=26.1 dB_m, StrtG=5.45, MaxG=342), Background average subtraction, Bandpass (Fc1=40 % Freq, Fp1=80 % Freq, Fp2=120 % Freq, Fc2=160 % Freq).





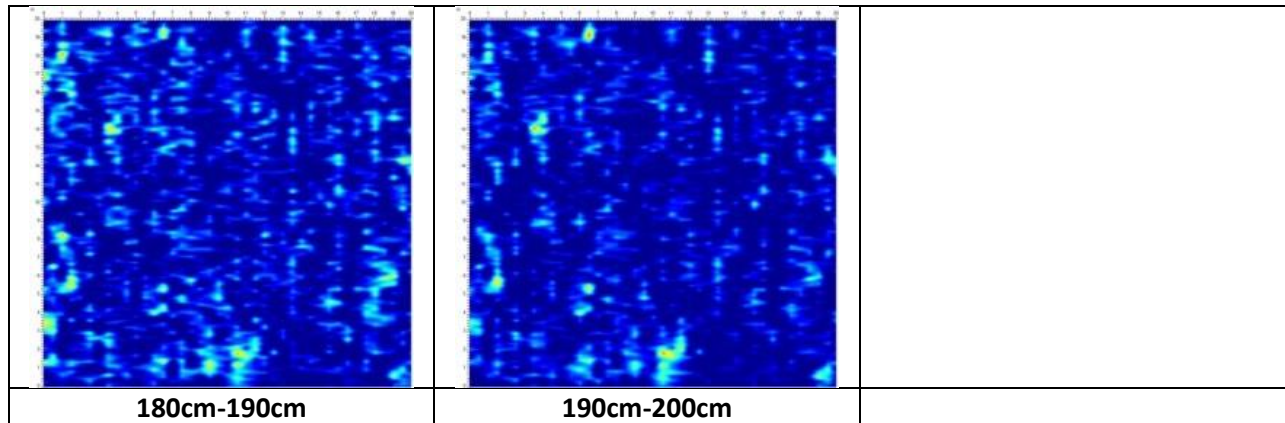
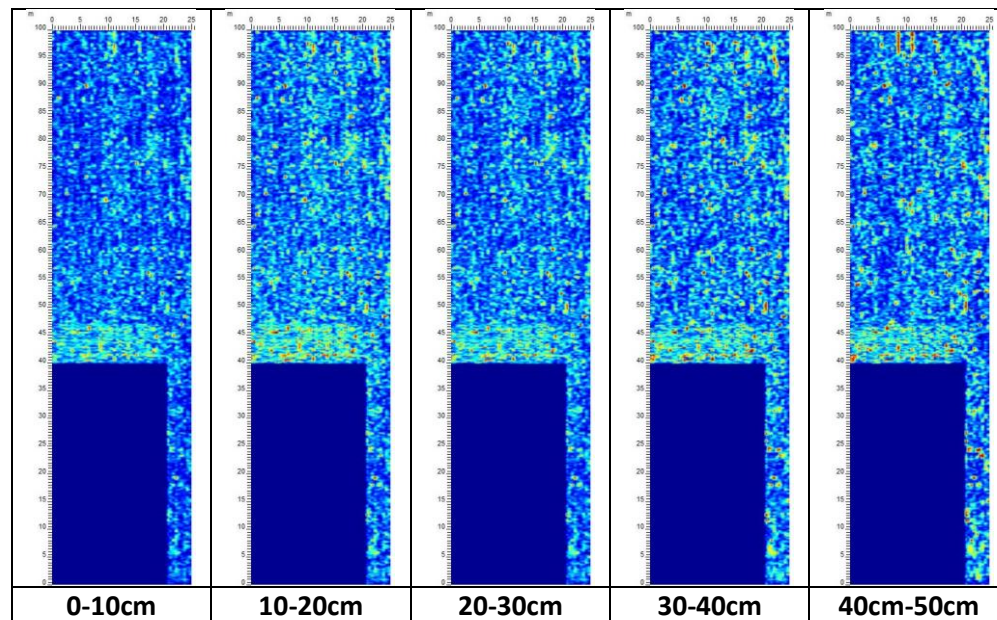
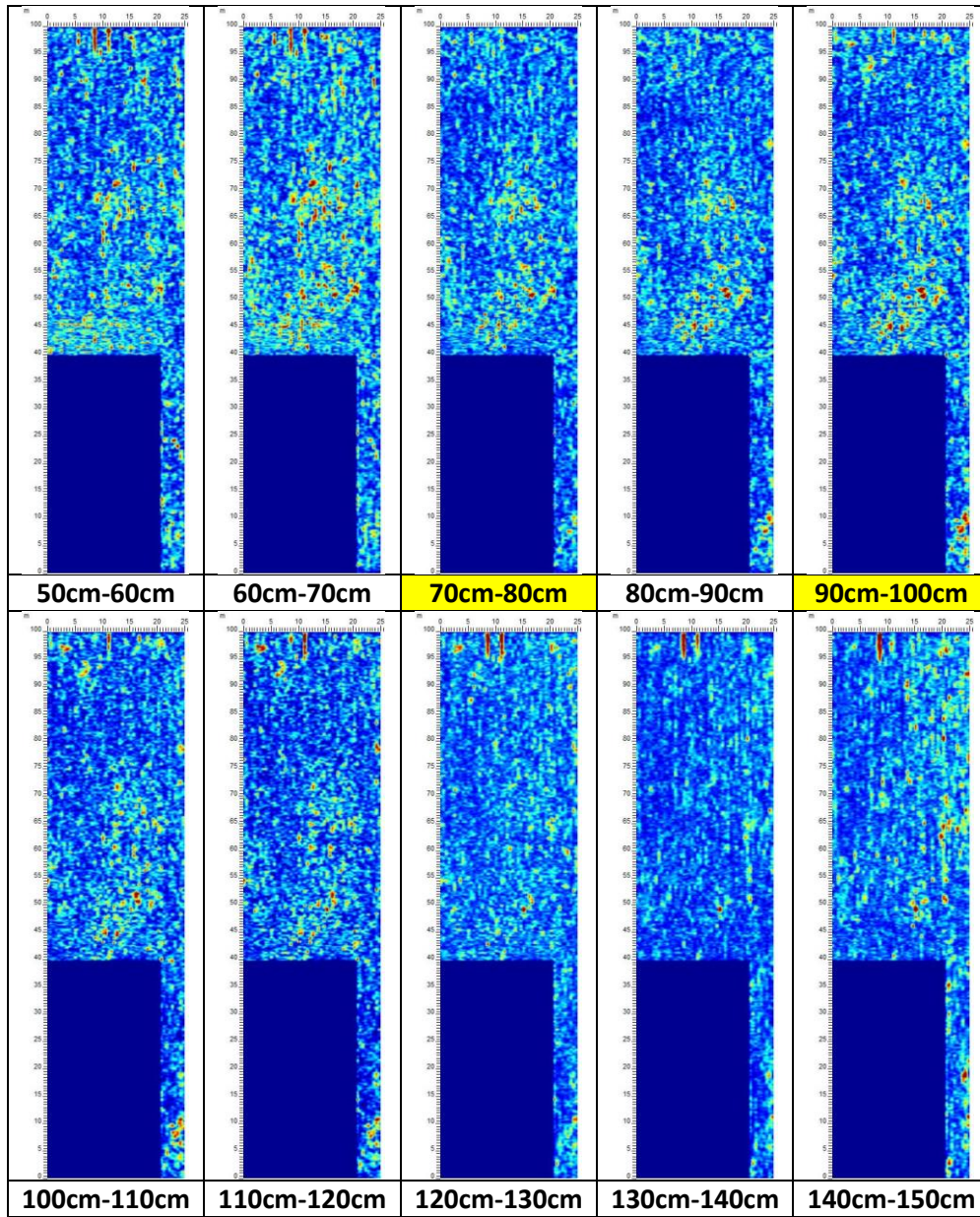


Table 1: GPR depth slices with 10cm thickness

GRID: RIZOMILOS2

Trace reposition, Repick first break (15%), Dewow, SEC2 (Atn=26.02 dB_m, StrtG=5.12, MaxG=400), Background average subtraction, Bandpass (Fc1=40 % Freq, Fp1=80 % Freq, Fp2=120 % Freq, Fc2=160 % Freq), Background removal (FW=15 m, Type=rectangular).





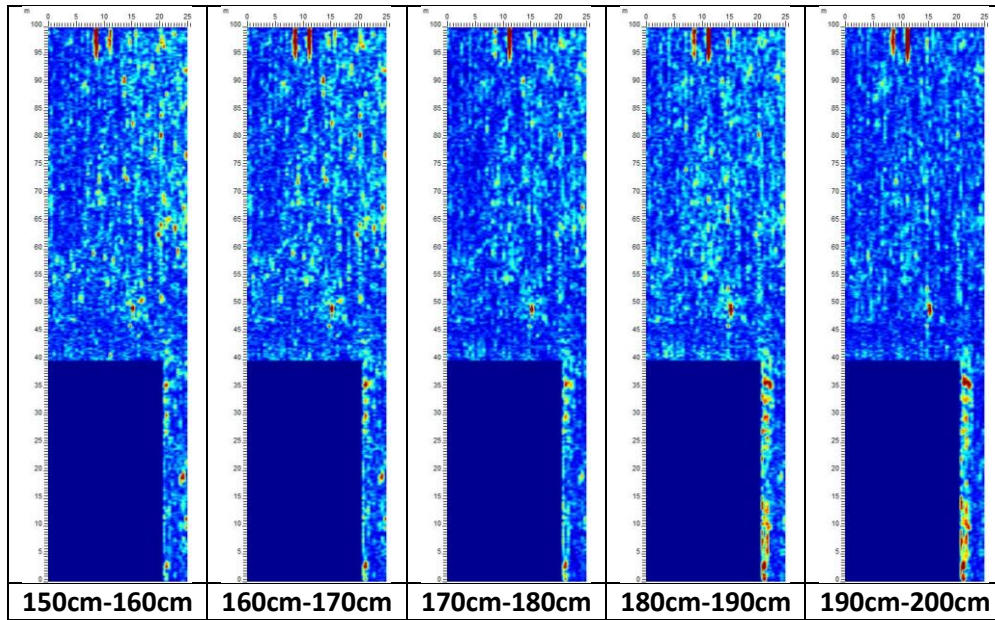
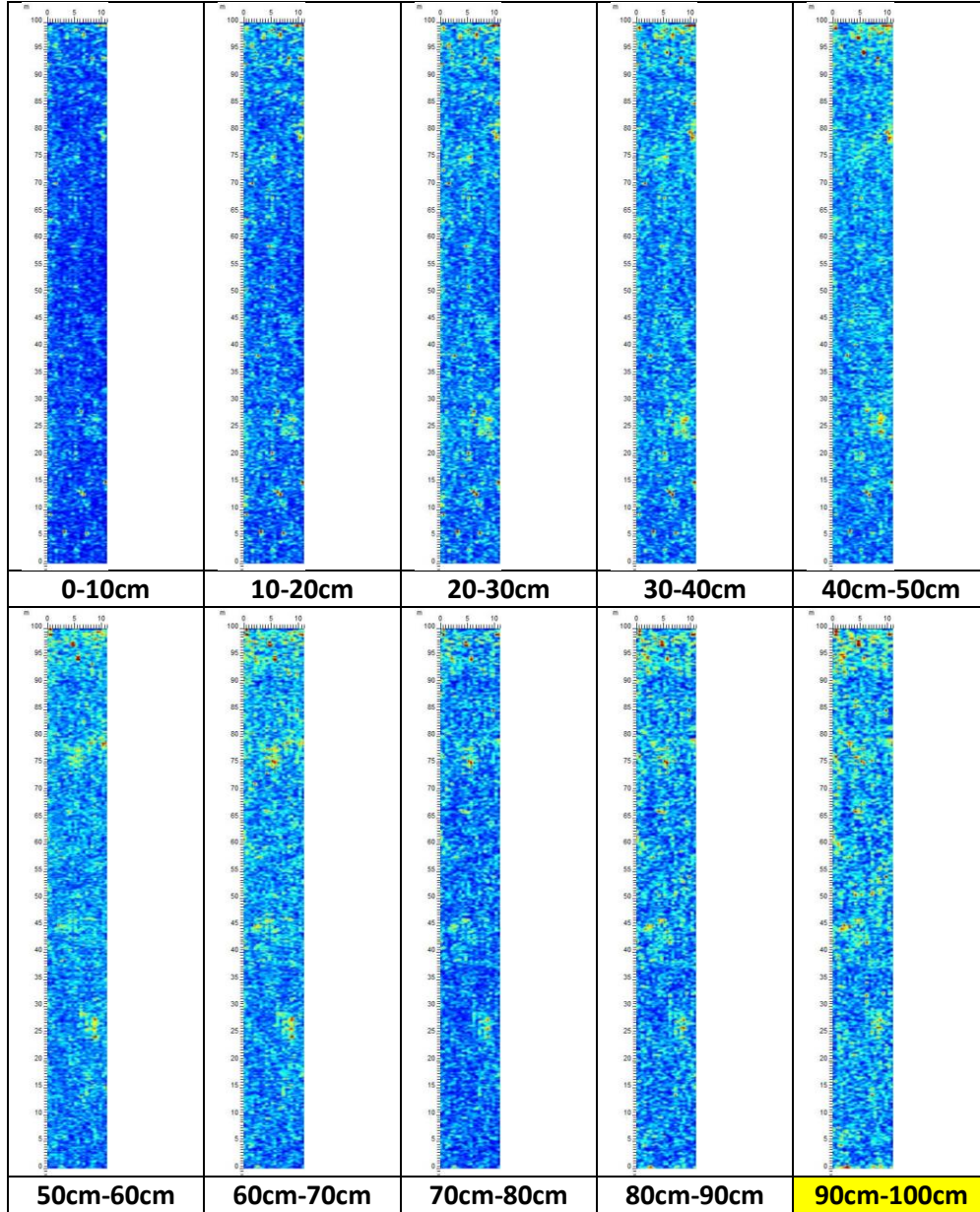


Table 2: GPR depth slices with 10cm thickness

GRID: RIZOMILOS3

Trace reposition, Repick first break (25%), Dewow, SEC2 (Atn=31.58 dB_m, StrtG=4.13, MaxG=227), Background average subtraction, Bandpass (Fc1=40 % Freq, Fp1=80 % Freq, Fp2=120 % Freq, Fc2=160 % Freq), Background removal (FW=3 m, Type=rectangular).



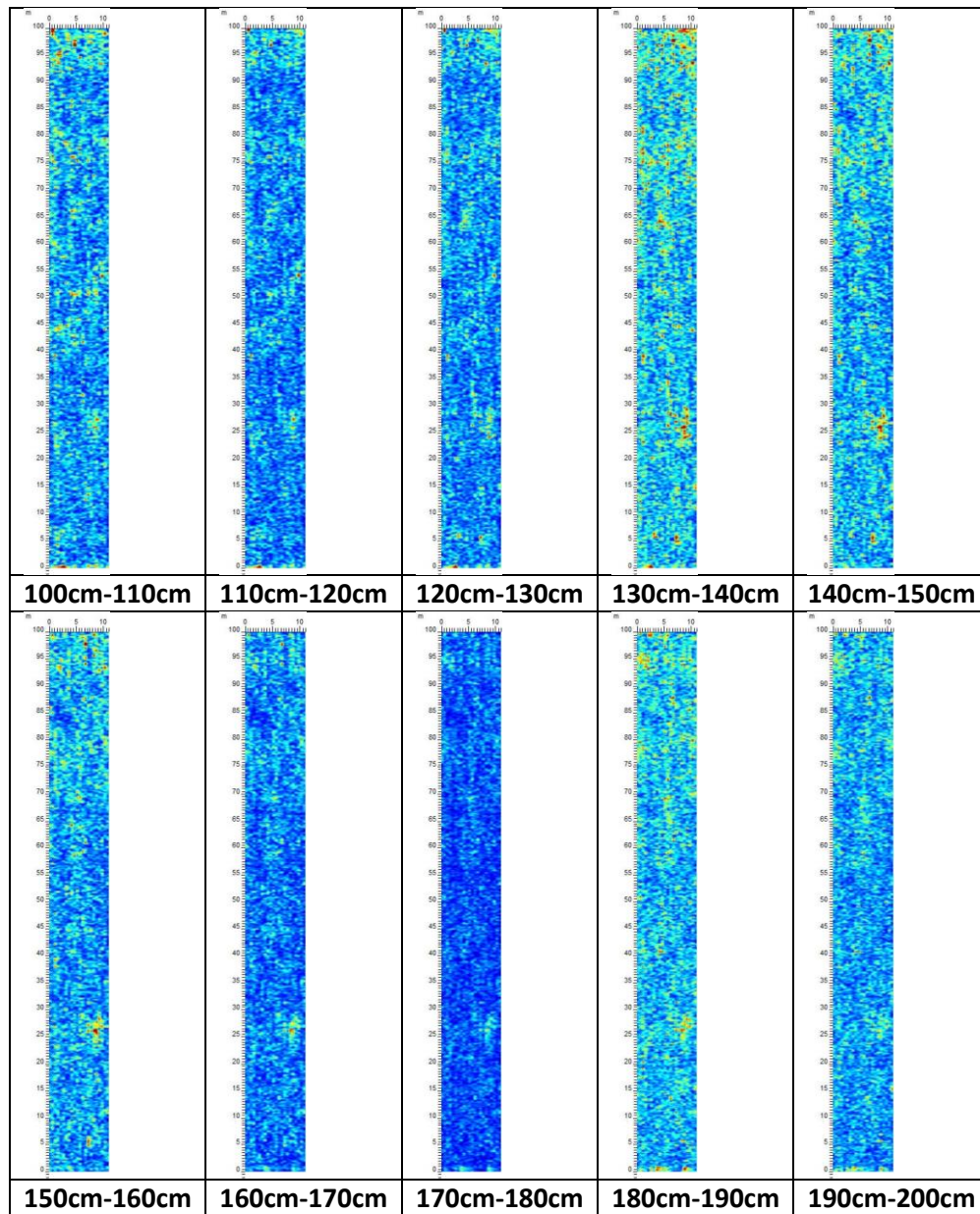


Table 3: GPR depth slices with 10cm thickness

Soil Studies

At the time of the soil sampling the crops were harvested and some of the fields presented burnt patches (A in Figure 19). A total of 3 lines were sampled across the site, targeting a series of concentric ditch-like positive magnetic anomalies (Line 1 and 2 in Figure 20) and similar linear ditch-like anomaly showing a positive magnetic contrast (Line 3 in Figure 20). The width of these ditches varied between 4-6m. The soil samples were collected at 2 depths: A (0.20-0.25m) and B (0.25-0.30m). A series of points were also sampled to a depth ~1m (Figure 21). The features augured neither seemed to have been bottomed at the depth reached by the auger nor solid rock was reached. A series of control samples were taken outside of the known site.

The mean value of the χ_{lf} measurements along the different lines was $\sim 1.55E-06$ for the A and B depth samples (Table 4). The mean χ_{lf} values inside magoula were increased by 59% and 53% than those from the control samples (off-site) taken at the same A and B depths respectively. The mean P value of all the lines sampled was 1804ppm whilst the off-site control samples sampled at the same depth was 292.07ppm.

MEAN VALUES & % INCREASE (LINE SAMPLES, RIZOMILOS)							
Analysis		Magnetic Susceptibility (χ_{lf} , $10^{-6} m^3 kg^{-1}$)				Phosphate (ppm)	
LINE	Length (m)	N ^o	A (0.20-0.25m)	N ^o	B (0.25-0.30m)	N ^o	B (0.25-0.30m)
1	133	24	1.50E-06	23	1.52E-06	22	2047.14
2	127	15	1.59E-06	16	1.57E-06	16	1590.89
3	52	14	1.55E-06	16	1.55E-06	16	1773.96
Mean		1.55E-06		1.55E-06		1804.00	
CONTROL		1	9.77E-07	1	1.01E-06	1	292.07
% Increase		58.54%		53.18%		517.66%	

Table 4: The table shows the mean values of the results of the low frequency MS (χ_{lf}) and P analyses (ppm=parts per millions) of the lines sampled at Rizomilos 2 at two depths (A & B) and the off-site control samples. The table also shows the total percentage increase in MS and P of the off-site/in-site samples.

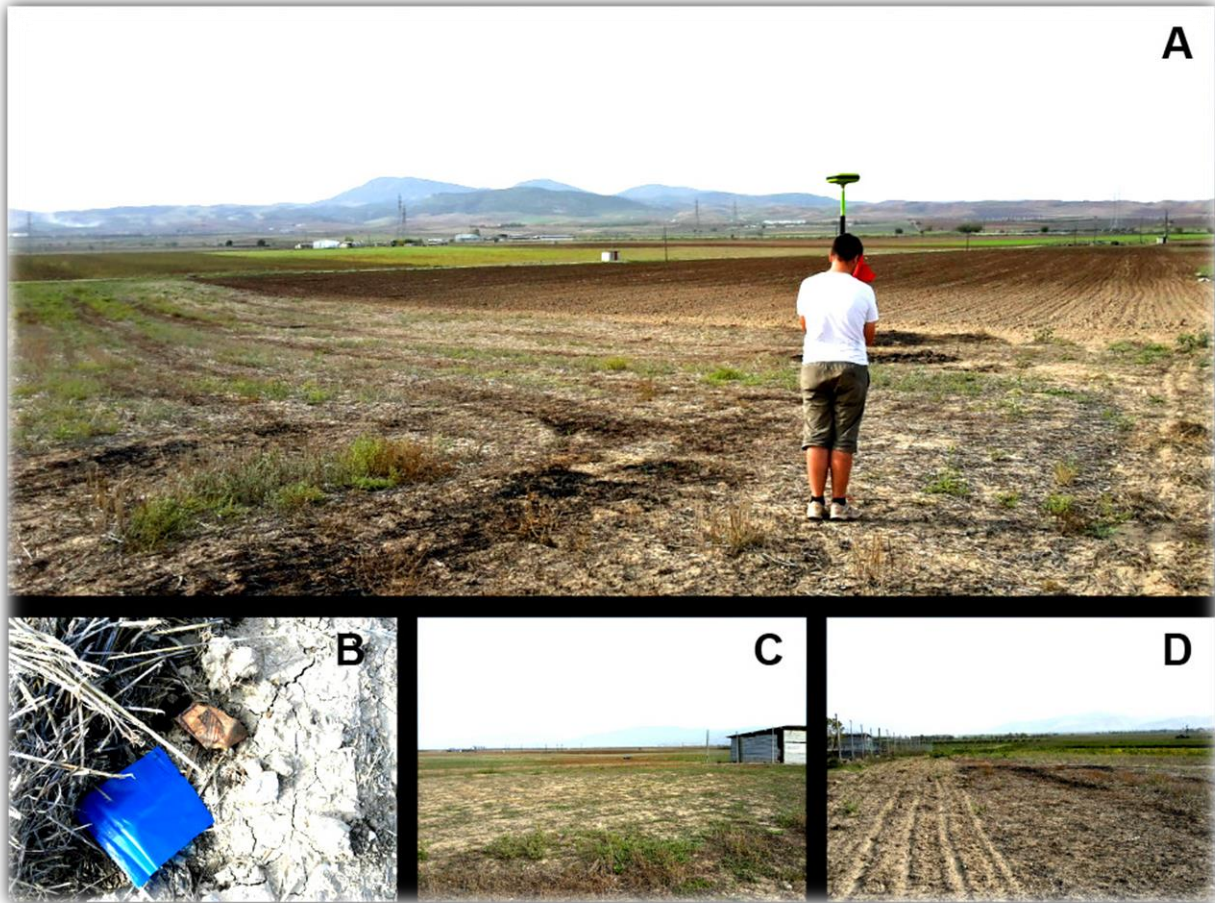


Figure 19: Different views from the top of Rizomilos 2 magoula during the soil sampling of Line 1 (Figure 14): surveying the soil samples and view of the fields at the SW and burnt crops patches (A), Neolithic surface potsherd (B) and NE views of the illegal farm at the top of the magoula (C & D)

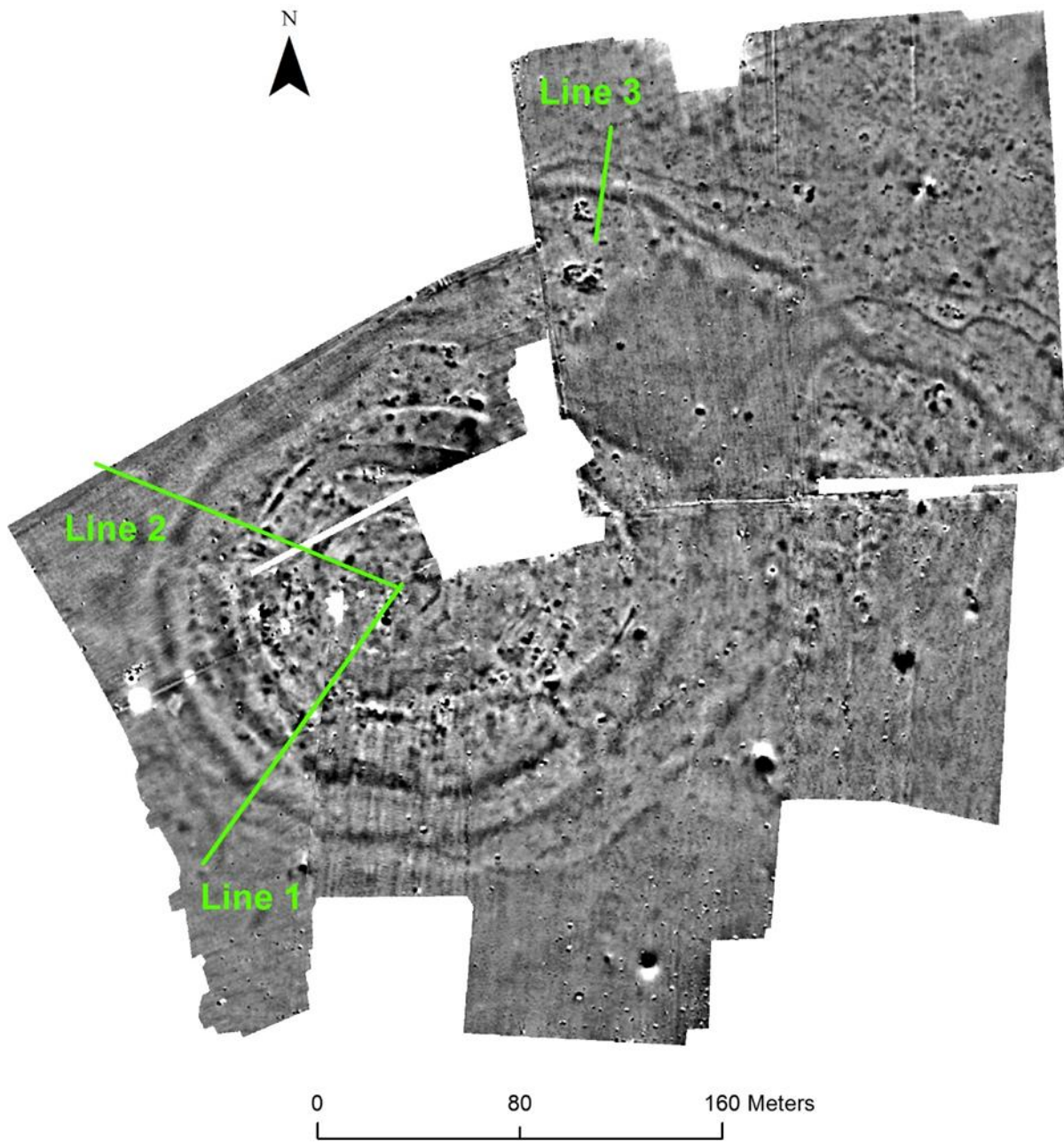


Figure 20: Location of the sampled lines (in green) at Rizomilos 2. The grey scale image shows the results of the magnetometer survey (positive magnetic anomalies are displayed in black and negative magnetic anomalies in white).

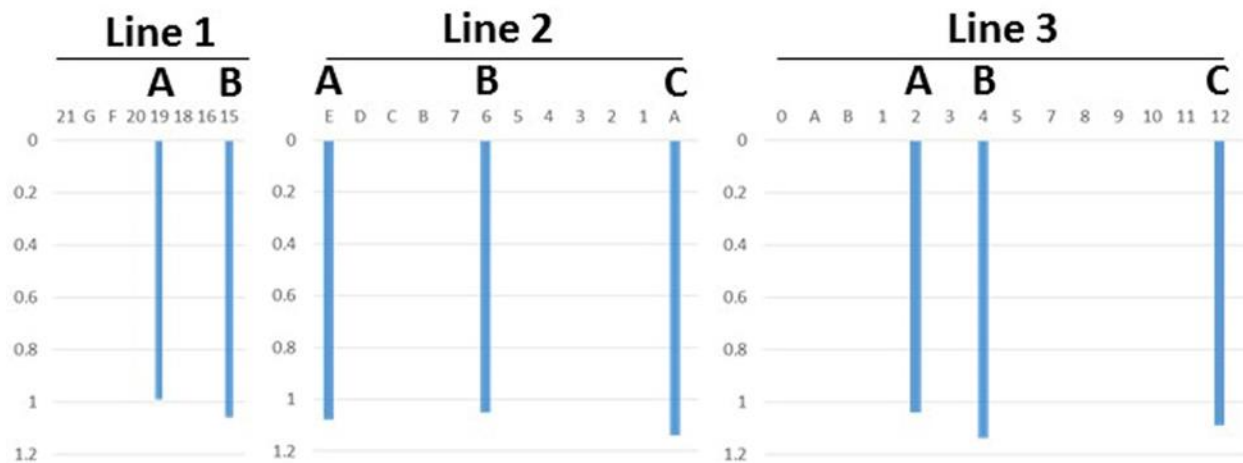
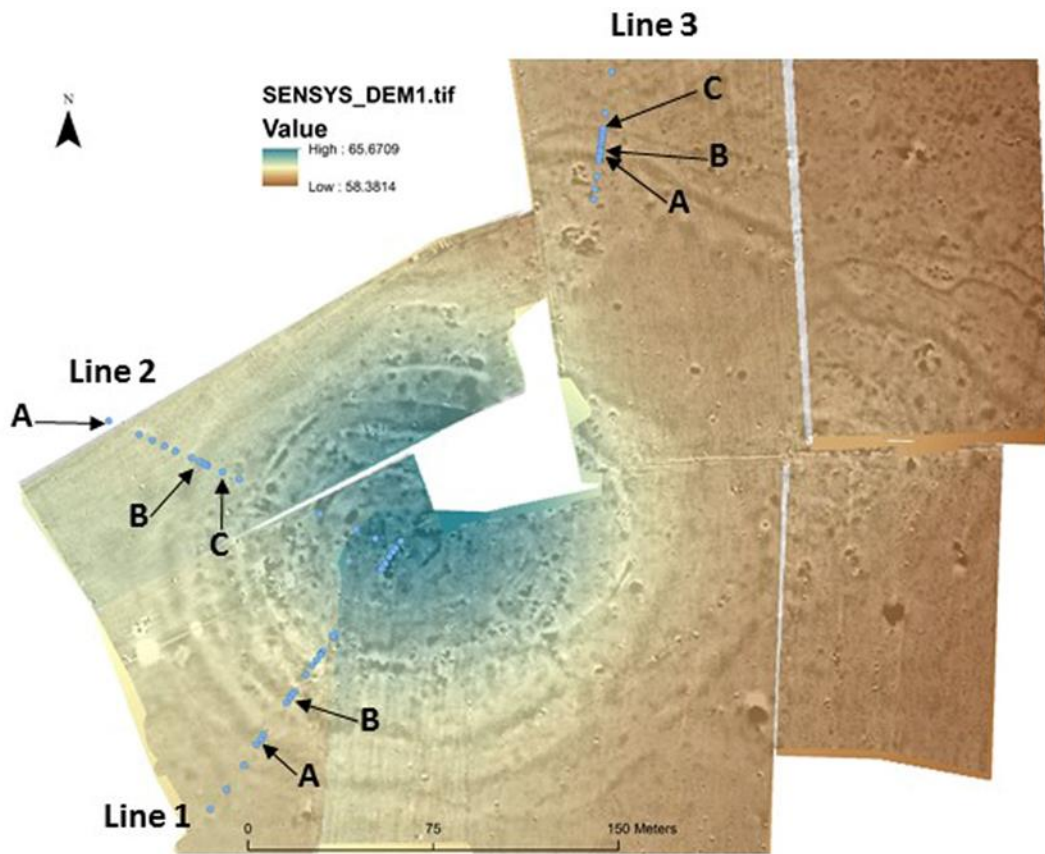


Figure 21: Location of the samples collected at Rizomilos 2 and the depths reached with the targeted ‘auger’ sampling. The grey scale image shows the results of the magnetometer survey (positive magnetic anomalies are displayed in black and negative magnetic anomalies in white). The image shows also the results of the digital elevation model (DEM) overlying the magnetometer results. The vertical axis in the graphs shows the depth from the surface in meters and the horizontal axis shows the code of the samples.

Line 1

The results of Line 1 are summarized in Table 5 and Table 6. The most significant observation of the lateral distribution of MS was its decreased values at the center of the magoula (Figure 22). The results of the 'auger' samples targeting the two concentric positive magnetic anomalies (A & B in Figure 22) showed enhanced values ($\sim 1.65\text{E-}06$) up to 0.54m depth in point A. Then, higher averaged values ($1.74\text{E-}06$) followed at least up to 0.95m. Point B showed enhanced χ_{lf} values ($1.70\text{E-}06$) up to 0.96m depth, with an averaged peak of $1.79\text{E-}06$ from 0.40 to 0.55m depth. The samples with highest MS values were those collected on and immediately close to the ditch-like positive magnetic anomalies revealed by the gradiometer survey. The lateral variation of the magnetic intensity and MS had a similar pattern (Figure 23).

The P analysis showed general increased values towards the center of the magoula as well as enhanced P to the east of the innermost ditch-like positive magnetic anomaly (2 in Figure 23). The P content variable presents a negative correlation with the MS at high and low frequencies (Figure 24).

LINE 1 (RIZOMILOS)							
Analysis	Magnetic Susceptibility						Phosphate
Depth	A (0.20-0.25m)			B (0.25-0.30m)			B (0.25-0.30m)
ID	χ_{lf}	χ_{hf}	FD (%)	χ_{lf}	χ_{hf}	FD (%)	(ppm)
0	1.24E-06	1.15E-06	6.76	1.23E-06	1.15E-06	6.32	2784.76
1	1.19E-06	1.13E-06	5.40	1.19E-06	1.12E-06	5.60	1928.69
2	1.16E-06	1.09E-06	5.95	1.04E-06	9.73E-07	6.56	3061.73
3	1.16E-06	1.08E-06	6.74	1.14E-06	1.06E-06	6.65	1941.28
4	1.17E-06	1.09E-06	6.56	1.22E-06	1.14E-06	6.36	2180.47
B	1.16E-06	1.09E-06	6.44				
5	1.65E-06	1.52E-06	7.65	1.53E-06	1.42E-06	6.98	1890.92
6	1.60E-06	1.48E-06	7.42	1.56E-06	1.45E-06	6.97	2130.12
7	1.58E-06	1.46E-06	7.36	1.62E-06	1.50E-06	7.46	2558.15
8	1.63E-06	1.51E-06	7.59	1.68E-06	1.55E-06	7.59	2016.81
9	1.63E-06	1.51E-06	7.73				
10	1.64E-06	1.51E-06	7.58	1.63E-06	1.51E-06	7.07	1941.28
11	1.63E-06	1.50E-06	7.74	1.65E-06	1.52E-06	7.42	2482.62
12	1.66E-06	1.53E-06	7.51	1.72E-06	1.59E-06	7.21	1853.15
C	1.47E-06	1.37E-06	7.30				
D				1.54E-06	1.43E-06	7.56	2230.83
13	1.68E-06	1.55E-06	7.65	1.71E-06	1.58E-06	7.42	3175.03
14	1.65E-06	1.65E-06		1.65E-06	1.52E-06	7.66	
15	1.73E-06	1.60E-06	7.85	1.73E-06	1.61E-06	6.72	1916.1
16	1.68E-06	1.55E-06	7.55	1.65E-06	1.52E-06	7.85	1865.74
18	1.65E-06	1.52E-06	7.73	1.66E-06	1.54E-06	7.18	1765.03
19	1.62E-06	1.50E-06	7.60	1.59E-06	1.48E-06	7.18	1689.49
20	1.54E-06	1.44E-06	6.93	1.65E-06	1.53E-06	7.27	1488.06
F	1.65E-06	1.53E-06	7.47	1.69E-06	1.57E-06	7.52	2167.88
G				1.72E-06	1.59E-06	7.47	1525.83
21	1.30E-06	1.20E-06	7.63	1.27E-06	1.18E-06	7.11	443.14
MIN	1.16E-06	1.08E-06	5.40	1.04E-06	9.73E-07	5.60	443.14
MAX	1.73E-06	1.65E-06	7.85	1.73E-06	1.61E-06	7.85	3175.03
MEAN	1.50E-06	1.40E-06	7.22	1.52E-06	1.42E-06	7.09	2047.14
S.D.	2.08E-07	1.92E-07	0.64	2.19E-07	1.98E-07	0.53	572.53
C.V.	13.85	13.71	8.84	14.36	14.01	7.42	27.97

Table 5: Results of the MS and P analyses of the soil sampled in Line 1 at Rizomilos at two different depths (A & B). The abbreviations stand for: low frequency MS (χ_{lf}), high frequency MS (χ_{hf}), frequency dependent percentage (fd%) and parts per million (ppm). The table also shows the minimum (MIN) and maximum (MAX) values, as well as the mean, standard deviation (S.D.) and coefficient of variation (C.V.) of the measurements.

PROFILE SAMPLES FROM LINE 1 (RIZOMILOS)											
Magnetic Susceptibility											
POINT A				POINT B				CONTROL			
Depth	χ_{lf}	χ_{hf}	FD (%)	DEPTH	χ_{lf}	χ_{hf}	FD (%)	DEPTH	χ_{lf}	χ_{hf}	FD (%)
0.22-0.26	1.73E-06	1.60E-06	7.85	0.20-0.25	1.62E-06	1.50E-06	7.60	0.19-0.25	9.77E-07	9.00E-07	7.88
0.26-0.31	1.73E-06	1.61E-06	6.72	0.25-0.3	1.59E-06	1.48E-06	7.18	0.24-0.32	1.01E-06	9.32E-07	7.90
0.31-0.36	1.71E-06	1.58E-06	7.50	0.3-0.34	1.72E-06	1.59E-06	7.09	0.31-0.36	9.23E-07	8.66E-07	6.10
0.36-0.42	1.64E-06	1.53E-06	6.70	0.34-0.40	1.69E-06	1.56E-06	7.51	0.36-0.42	9.34E-07	8.66E-07	7.23
0.42-0.48	1.70E-06	1.58E-06	7.42	0.40-0.47	1.62E-06	1.50E-06	7.36	0.42-0.47	9.07E-07	8.46E-07	6.64
0.48-0.56	1.79E-06	1.66E-06	7.23	0.47-0.53	1.65E-06	1.52E-06	7.88	0.47-0.54	9.14E-07	8.52E-07	6.81
0.56-0.62	1.79E-06	1.67E-06	6.60	0.53-0.54	1.65E-06	1.52E-06	7.76	0.5-0.20	9.73E-07	8.99E-07	7.62
0.62-0.68	1.56E-06	1.46E-06	6.50	0.54-0.63	1.75E-06	1.62E-06	7.77	0.54-0.60	8.99E-07	8.40E-07	6.55
0.68-0.79	1.70E-06	1.59E-06	6.72	0.63-0.72	1.69E-06	1.56E-06	7.95	0.60-0.62	8.79E-07	8.21E-07	6.70
0.79-0.9	1.67E-06	1.55E-06	7.06	0.72-0.8	1.75E-06	1.62E-06	7.46	0.62-0.68	8.79E-07	8.23E-07	6.38
0.9-0.96	1.66E-06	1.53E-06	7.69	0.80-0.87	1.74E-06	1.60E-06	7.59	0.68-0.80	8.17E-07	7.69E-07	5.85
0.97-1.06	1.532E-06	1.42E-06	7.52	0.87-0.95	1.7668E-06	1.64E-06	7.34	0.80-0.88	8.26E-07	7.74E-07	6.23
				0.95-0.99	1.7581E-06	1.64E-06	6.64	0.88-0.96	8.44E-07	7.94E-07	5.90
								0.96-1.02	8.43E-07	8.01E-07	5.02
MIN	1.53E-06	1.42E-06	6.50		1.59E-06	1.48E-06	6.64		8.17E-07	7.69E-07	5.02
MAX	1.79E-06	1.67E-06	7.85		1.77E-06	1.64E-06	7.95		1.01E-06	9.32E-07	7.90
MEAN	1.68E-06	1.56E-06	7.03		1.69E-06	1.57E-06	7.56		9.02E-07	8.42E-07	6.63
S.D.	7.90E-08	7.38E-08	0.47		6.0662E-08	5.77E-08	0.36		5.9059E-08	4.86E-08	0.82
C.V.	4.69	4.72	6.70		3.58	3.69	4.76		6.55	5.78	12.39

Table 6: Results of the MS analysis of the auger samples from Line 1 and the off-site controls collected at Rizomilos. The abbreviations stand for: low frequency MS (χ_{lf}), high frequency MS (χ_{hf}), frequency dependent percentage (fd%) and parts per million (ppm). The table also shows the minimum (MIN) and maximum (MAX) values, as well as the mean, standard deviation (S.D.) and coefficient of variation (C.V.) of the measurements.

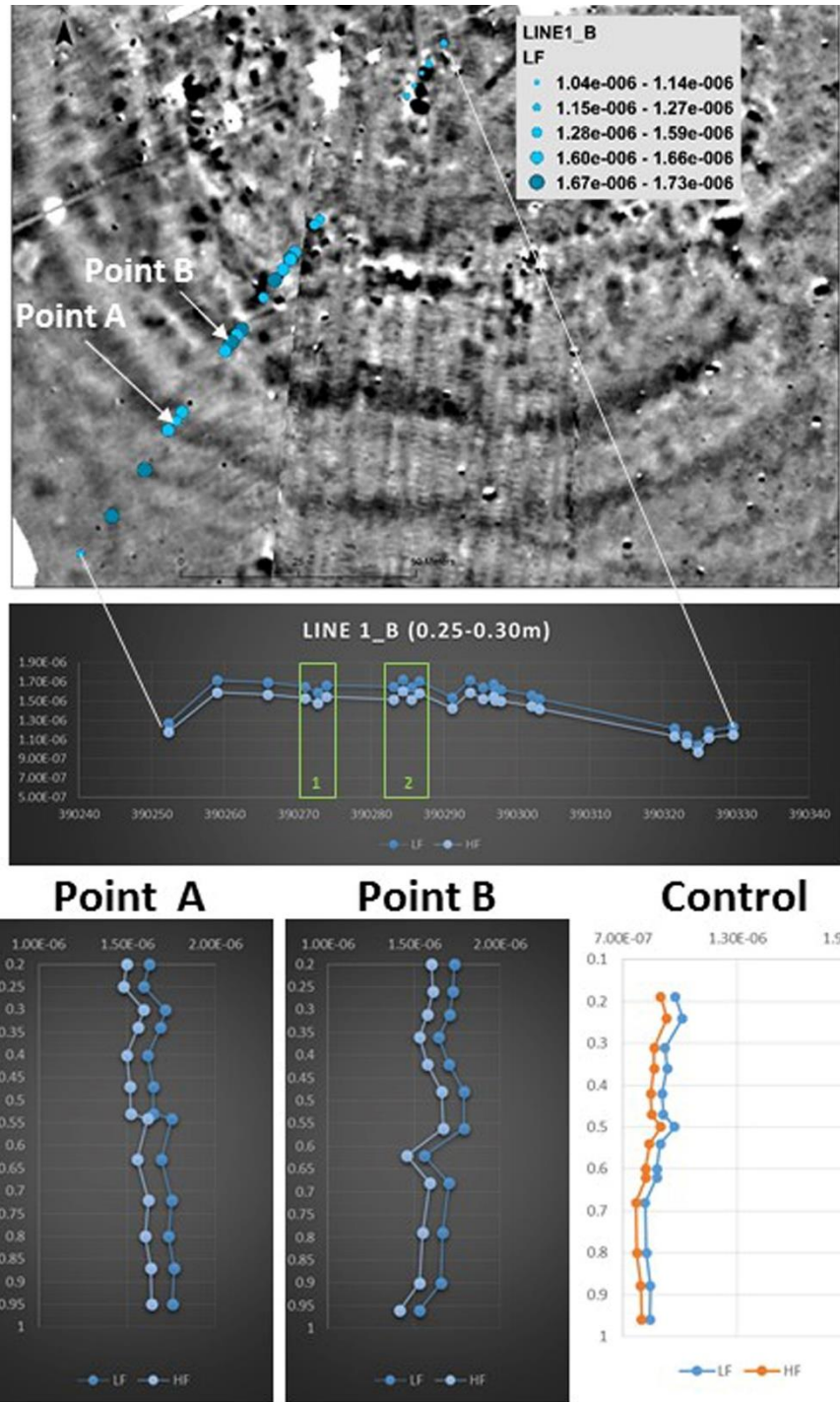


Figure 22: Bubble plot (above) and graph (middle) showing the lateral MS distribution along Line 1_B (Rizomilos 2). In the graph, the location of the two targeted ditch-like positive magnetic anomalies is indicated in green (1 & 2). The location and results of the 'auger' samples are also shown (A, B & off-site control).

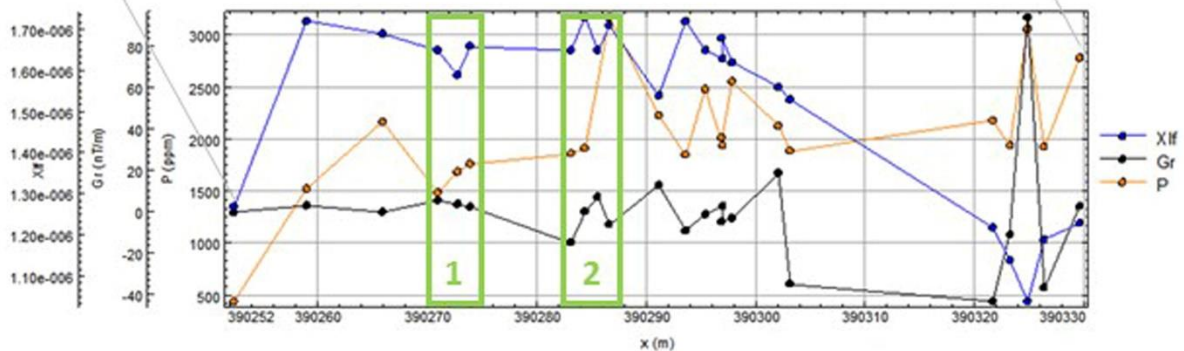
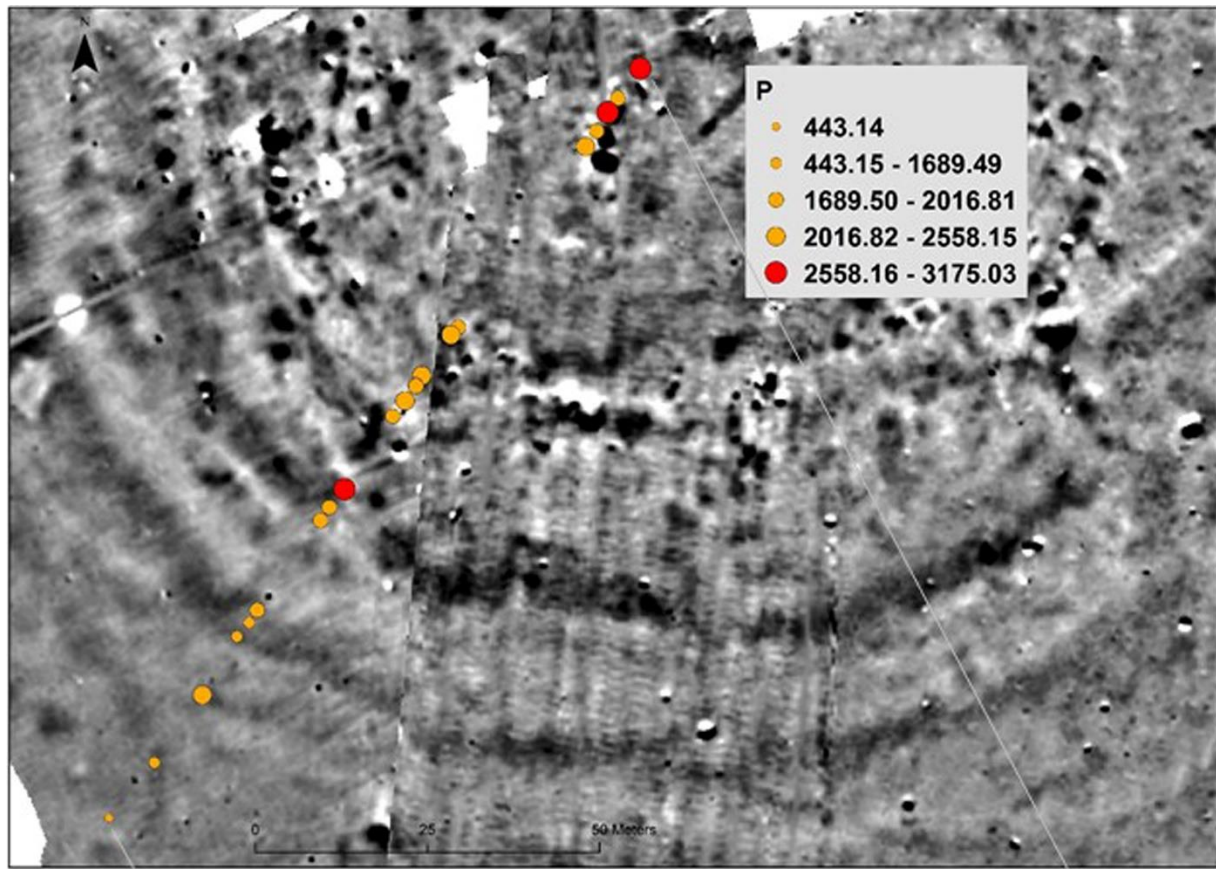


Figure 23: Bubble plot (above) showing the lateral P distribution along Line 1_B (Rizomilos 2). The graph (below) shows the lateral variation of the magnetic intensity (Gr), MS (X_{lf}) and P content. In the graph, the location of the two targeted ditch-like positive magnetic anomalies is indicated in green (1 & 2).

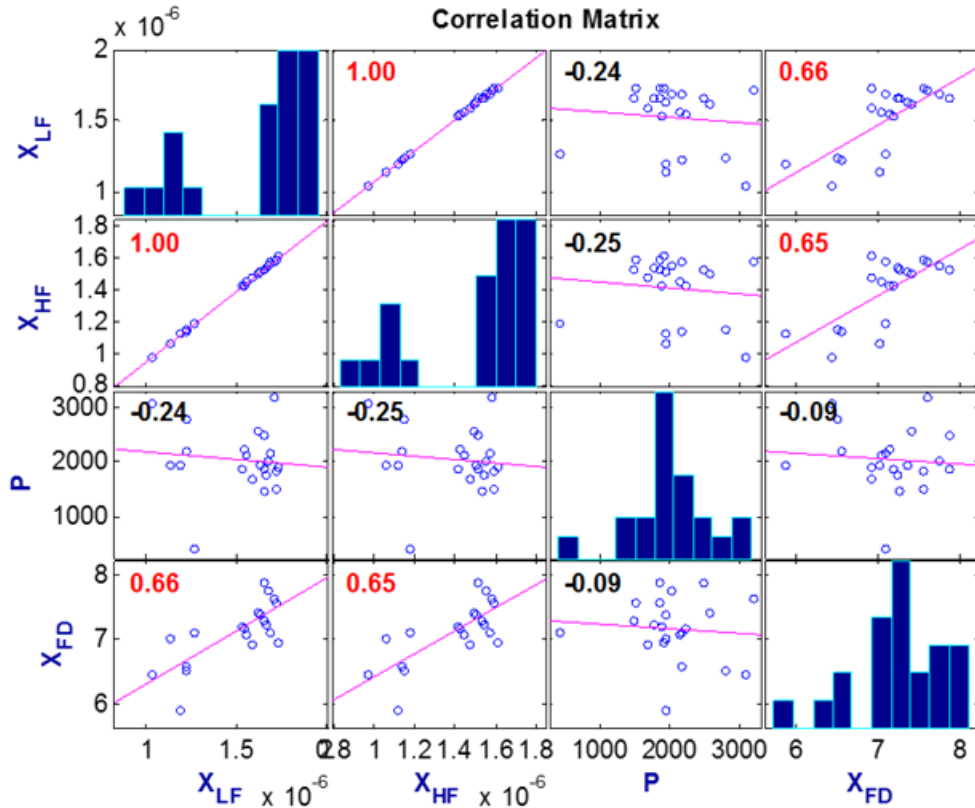


Figure 24: Results of the Spearman correlation (Line1_B, Rizomilos 2)

Line 2

Tables 7 and 8 show the results of Line 2. As in Line 1, they showed a clear decrease of MS values at the top of the magoula. There samples taken in the area with the ditch-like enclosures had increased MS values and the highest values where those sampled at the location of the innermost ditch (1 in Figure 19). Enhanced mean χ_{HF} values of $\sim 1.77E-06$ were measured in the ‘auger’ samples taken from point B at least up to 1.05m (Figure 25). The highest intensities of the magnetic gradient coincided with the location of the two possible ditch-enclosures (0 and 1 in Figure 26).

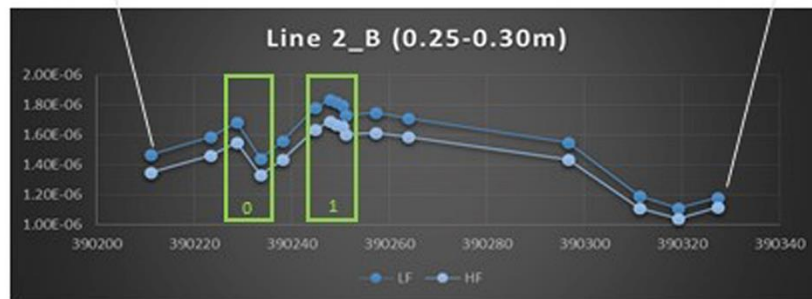
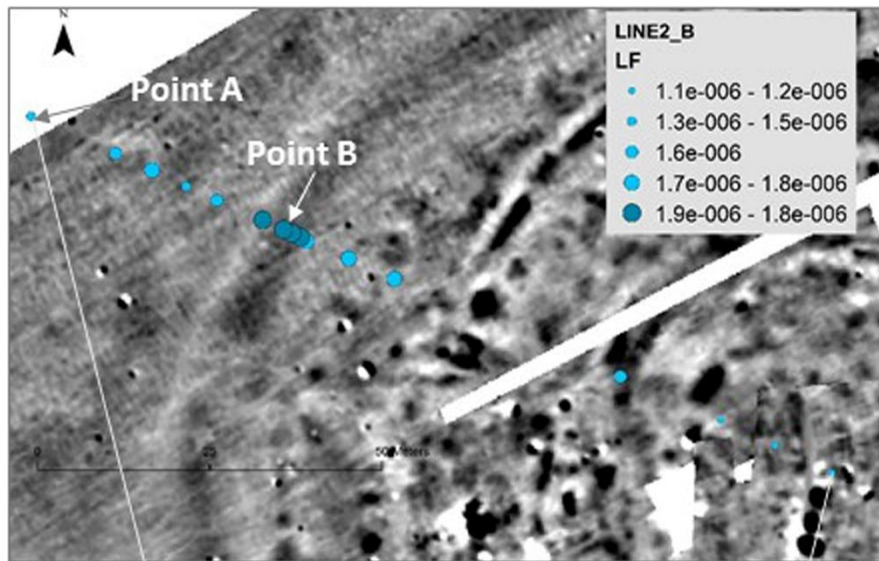
There was a steady increase of P content toward the center of the magoula (Figure 26). The high P value obtained from the outermost sample of line 2 may be related to analytical error or a mistake during the soil sampling. There is another high P value that correlates with another peak in the intensity of the magnetic gradient (Figure 26). This peak is located at an area where other narrower, linear and generally strong magnetic anomalies were detected. The P content also showed a negative correlation with the MS at high and low frequencies (Figure 27).

LINE 2 (RIZOMILOS)							
Analysis	Magnetic Susceptibility						Phosphate
Depth	A (0.20-0.25m)			B (0.25-0.30m)			B (0.25-0.30m)
ID	χ_{lf}	χ_{hf}	FD (%)	χ_{lf}	χ_{hf}	FD (%)	(ppm)
-A	1.23E-06	1.15E-06	6.32	1.18E-06	1.11E-06	5.82	1903.51
-B				1.11E-06	1.04E-06	6.32	2070.93
-C	1.18E-06	1.09E-06	6.92	1.19E-06	1.11E-06	6.85	2277.05
-D	1.17E-06	1.10E-06	6.41	1.55E-06	1.44E-06	7.30	3242.55
0	1.81E-06	1.66E-06	7.96	1.71E-06	1.58E-06	7.70	1810.58
A	1.71E-06	1.58E-06	7.29	1.75E-06	1.61E-06	7.86	1550.22
1	1.83E-06	1.70E-06	7.05	1.73E-06	1.60E-06	7.70	1582.76
2				1.79E-06	1.66E-06	7.69	1513.24
3	1.75E-06	1.62E-06	7.94	1.82E-06	1.67E-06	8.10	405.38
4	1.80E-06	1.66E-06	7.89	1.83E-06	1.69E-06	7.97	1488.06
5	1.77E-06	1.63E-06	8.00				
6	1.75E-06	1.61E-06	7.94	1.78E-06	1.63E-06	8.11	1127.13
7	1.55E-06	1.43E-06	7.64	1.56E-06	1.44E-06	7.86	493.50
C	1.66E-06	1.53E-06	7.73	1.44E-06	1.33E-06	7.30	2696.64
B				1.68E-06	1.55E-06	8.16	355.019
D	1.51E-06	1.39E-06	8.04	1.58E-06	1.46E-06	7.69	584.72
E	1.48E-06	1.36E-06	7.86	1.46E-06	1.35E-06	8.10	2352.99
MIN	1.17E-06	1.09E-06	6.32	1.11E-06	1.04E-06	5.82	355.02
MAX	1.83E-06	1.70E-06	8.04	1.83E-06	1.69E-06	8.16	3242.55
MEAN	1.59E-06	1.47E-06	7.50	1.57E-06	1.45E-06	7.53	1590.89
S.D.	2.41E-07	2.17E-07	0.60	2.38E-07	2.13E-07	0.67	847.02
C.V.	15.17	14.81	7.95	15.10	14.61	8.96	53.24

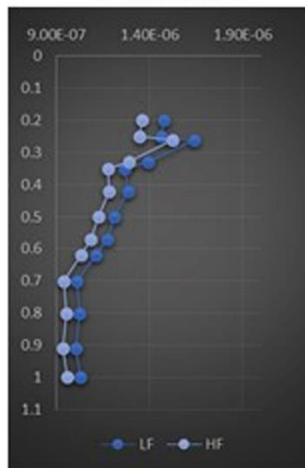
Table 7: Results of the MS and P analyses of the soil sampled in Line 2 at Rizomilos at two different depths (A & B). The abbreviations stand for: low frequency MS (χ_{lf}), high frequency MS (χ_{hf}), frequency dependent percentage (fd%) and parts per million (ppm). The table also shows the minimum (MIN) and maximum (MAX) values, as well as the mean, standard deviation (S.D.) and coefficient of variation (C.V.) of the measurements.

PROFILE SAMPLES FROM LINE 2 (RIZOMILOS)											
Magnetic Susceptibility											
POINT A				POINT B				CONTROL			
Depth	χ_{lf}	χ_{hf}	FD (%)	DEPTH	χ_{lf}	χ_{hf}	FD (%)	DEPTH	χ_{lf}	χ_{hf}	FD (%)
0.20-0.25	1.71E-06	1.58E-06	7.29	0.20-0.25	1.77E-06	1.63E-06	8.00	0.19-0.25	9.77E-07	9.00E-07	7.88
0.25-0.30	1.75E-06	1.61E-06	7.70	0.33-0.36	1.82E-06	1.67E-06	8.13	0.24-0.32	1.01E-06	9.32E-07	7.90
0.30-0.40	1.16E-06	1.09E-06	6.33	0.36-0.43	1.81E-06	1.67E-06	7.54	0.31-0.36	9.23E-07	8.66E-07	6.10
0.4-0.49	1.13E-06	1.06E-06	6.83	0.43-0.46	1.78E-06	1.64E-06	7.69	0.36-0.42	9.34E-07	8.66E-07	7.23
0.49-0.60	1.22E-06	1.13E-06	6.90	0.46-0.54	1.81E-06	1.66E-06	8.19	0.42-0.47	9.07E-07	8.46E-07	6.64
0.60-0.69	1.19E-06	1.11E-06	6.31	0.58-0.74	1.81E-06	1.66E-06	8.37	0.47-0.54	9.14E-07	8.52E-07	6.81
0.69-0.85	1.19E-06	1.11E-06	6.46	0.74-0.86	1.81E-06	1.66E-06	8.33	0.5-0.20	9.73E-07	8.99E-07	7.62
0.85-0.98	1.20E-06	1.13E-06	5.94	0.86-0.95	1.81E-06	1.66E-06	8.28	0.54-0.60	8.99E-07	8.40E-07	6.55
0.98-1.14	1.18E-06	1.11E-06	6.28	0.95-1.05	1.73E-06	1.59E-06	8.10	0.60-0.62	8.79E-07	8.21E-07	6.70
								0.62-0.68	8.79E-07	8.23E-07	6.38
								0.68-0.80	8.17E-07	7.69E-07	5.85
								0.80-0.88	8.26E-07	7.74E-07	6.23
								0.88-0.96	8.44E-07	7.94E-07	5.90
								0.96-1.02	8.43E-07	8.01E-07	5.02
MIN	1.13E-06	1.06E-06	5.94	1.73E-06	1.59E-06	7.54	8.17E-07	7.69E-07	5.02		
MAX	1.75E-06	1.61E-06	7.70	1.82E-06	1.67E-06	8.37	1.01E-06	9.32E-07	7.90		
MEAN	1.30E-06	1.21E-06	6.67	1.79E-06	1.65E-06	8.07	9.02E-07	8.42E-07	6.63		
S.D.	2.43E-07	2.19E-07	0.56	2.8673E-08	2.58E-08	0.28	5.9059E-08	4.86E-08	0.82		
C.V.	18.63	18.03	8.38	1.60	1.56	3.53	6.55	5.78	12.39		

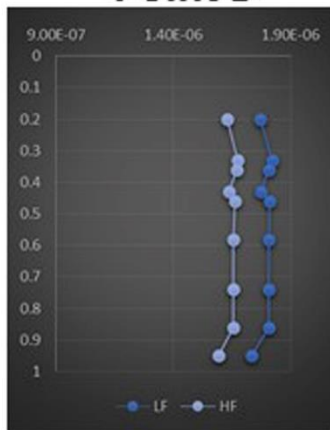
Table 8: Results of the MS analysis of the auger samples from Line 2 and the off-site controls collected at Rizomilos 2. The abbreviations stand for: low frequency MS (χ_{lf}), high frequency MS (χ_{hf}), frequency dependent percentage (fd%) and parts per million (ppm). The table also shows the minimum (MIN) and maximum (MAX) values, as well as the mean, standard deviation (S.D.) and coefficient of variation (C.V.) of the measurements.



Point A



Point B



Control

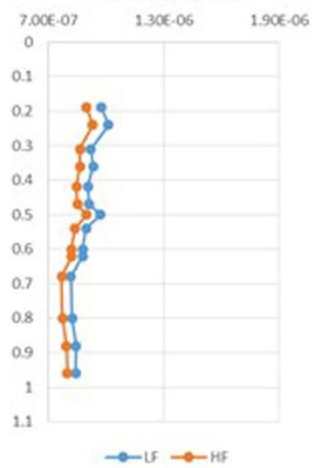


Figure 25: Bubble plot (above) and graph (middle) showing the lateral MS distribution along Line 2_B (Rizomilos 2). In the graph, the location of the two targeted ditch-like positive magnetic anomalies is indicated in green (0 & 1). The location and results of the 'auger' samples are also shown (A, B & off-site Control).

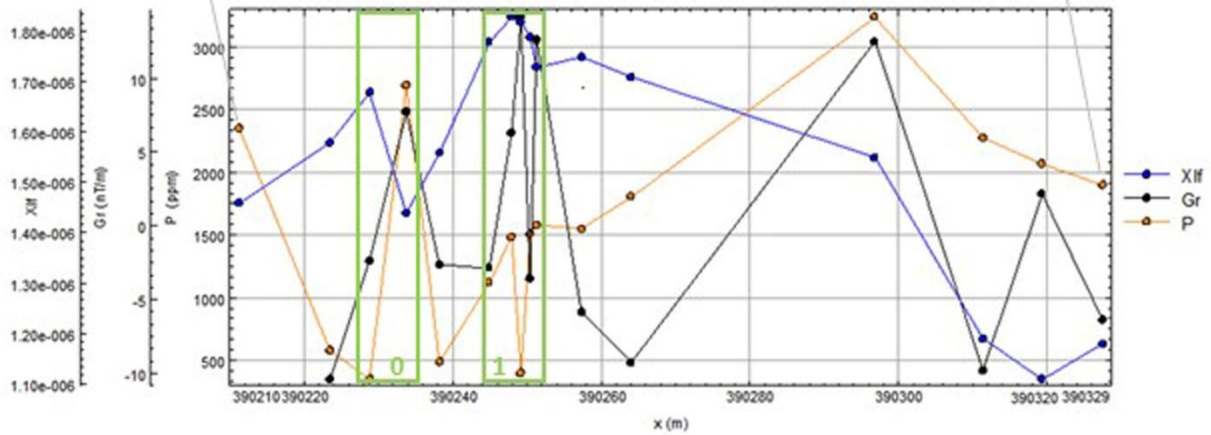
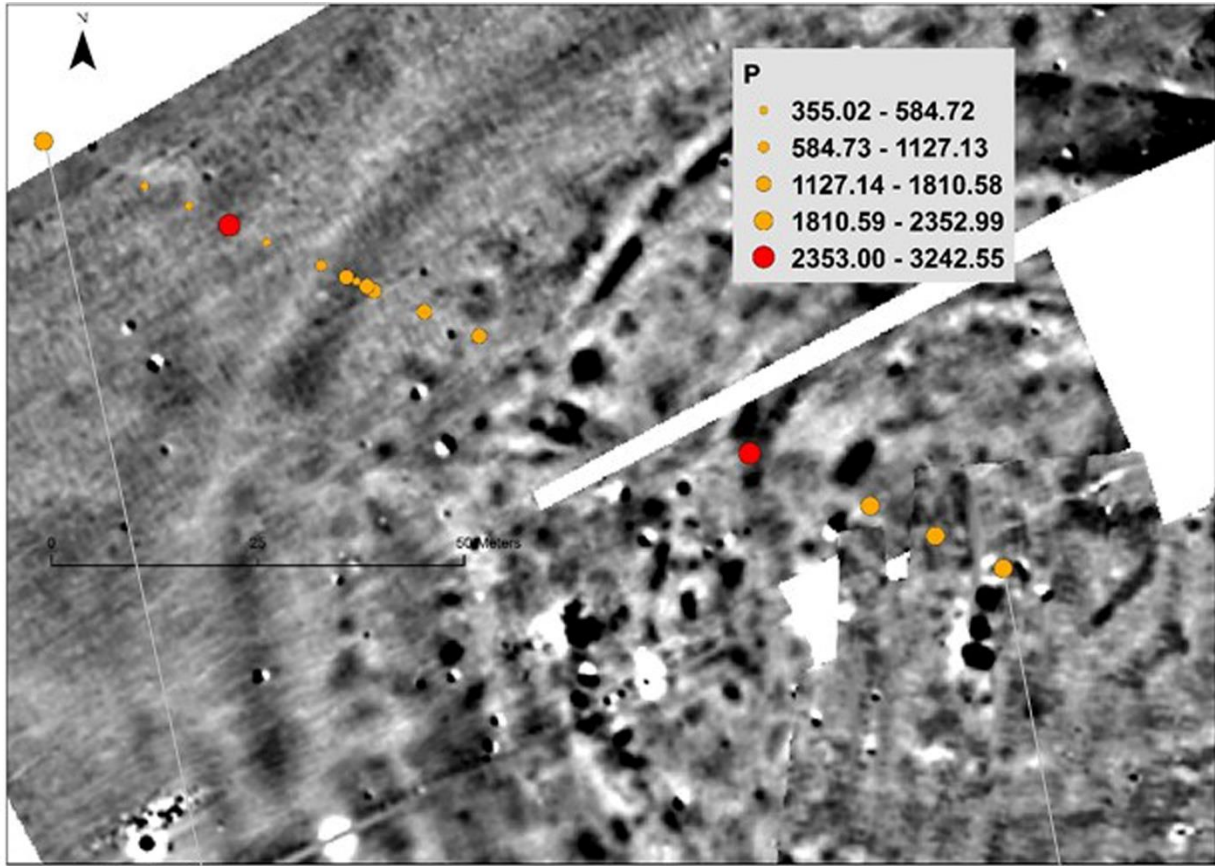


Figure 26: Bubble plot (above) showing the lateral P distribution along Line 2_B (Rizomilos 2). The graph (below) shows the lateral variation of the magnetic intensity (Gr), MS (X_{lf}) and P content. In the graph, the location of the two targeted ditch-like positive magnetic anomalies is indicated in green (0 & 1).

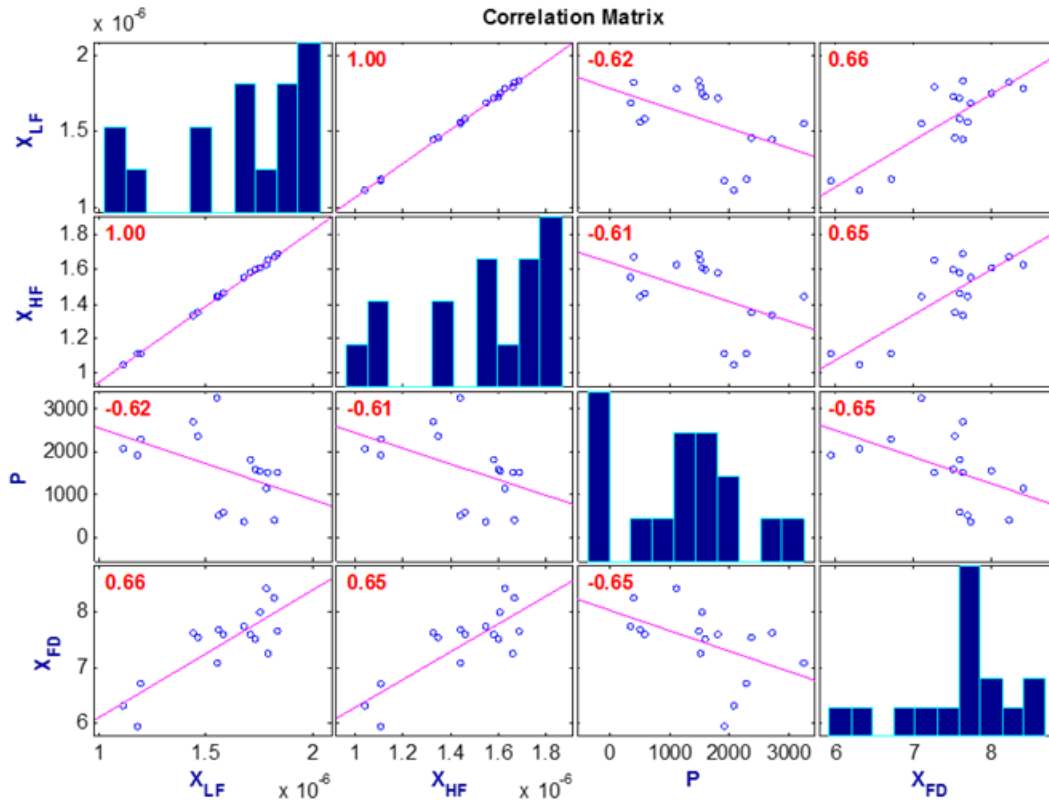


Figure 27: Results of the Spearman correlation (Line2_B, Rizomilos 2)

Line 3

The results of Line 3 are shown in Tables 9 and 10. Unlike Line 1 and 2, the MS results showed a general increase towards the magoula (Figure 28). The samples taken inside the targeted ditch-like magnetic anomaly (point A taken within the positive magnetic anomaly) showed enhanced χ_f values $\sim 1.53E-06$; up to 0.47m. Point B (located in the negative magnetic halo of the targeted anomaly) also showed averaged values of $1.51E-06$ up to 0.52m depth. The enhanced values obtained from the backfills of this specific feature were $\sim 15\%$ lower than the ditch-like features targeted in Line 1 and 2.

The highest intensities of the magnetic gradient coincided with the center of the ditch-like anomaly but do not correlate to the general increasing pattern of the MS results (Figure 29). The results of the P analysis showed a general increase towards the center of the magoula (Figure 29) and a strong correlation with the MS results (Figure 30).

LINE 3 (RIZOMILOS)							
Analysis	Magnetic Susceptibility						Phosphate
Depth	A (0.20-0.25m)			B (0.25-0.30m)			B (0.25-0.30m)
ID	χ_{lf}	χ_{hf}	FD (%)	χ_{lf}	χ_{hf}	FD (%)	(ppm)
0	1.59E-06	1.47E-06	7.64	1.63E-06	1.51E-06	7.51	2971.34
A	1.59E-06	1.46E-06	7.99	1.61E-06	1.48E-06	7.82	2005.84
B	1.64E-06	1.52E-06	7.65	1.61E-06	1.48E-06	8.06	1723.79
1	1.65E-06	1.53E-06	7.61	1.57E-06	1.45E-06	7.38	1940.75
2				1.57E-06	1.45E-06	7.81	1539.37
3	1.60E-06	1.48E-06	7.64	1.61E-06	1.49E-06	7.56	1691.24
4	1.49E-06	1.38E-06	7.95	1.57E-06	1.45E-06	7.09	1984.15
5				1.56E-06	1.45E-06	6.30	1571.91
6	1.55E-06	1.44E-06	6.78	1.57E-06	1.45E-06	7.82	1810.58
7	1.56E-06	1.43E-06	7.91	1.61E-06	1.49E-06	7.40	2092.63
8	1.57E-06	1.44E-06	7.80	1.54E-06	1.42E-06	7.73	2255.35
9	1.55E-06	1.43E-06	7.78	1.55E-06	1.43E-06	7.78	1615.31
10	1.56E-06	1.45E-06	6.97	1.51E-06	1.40E-06	7.22	1322.40
11	1.49E-06	1.37E-06	7.64	1.52E-06	1.41E-06	7.18	1528.52
C	1.47E-06	1.35E-06	7.90	1.50E-06	1.38E-06	7.69	1322.40
D	1.38E-06	1.27E-06	7.78	1.33E-06	1.22E-06	8.56	1007.80
MIN	1.38E-06	1.27E-06	6.78	1.33E-06	1.22E-06	6.30	1.01E+03
MAX	1.65E-06	1.53E-06	7.99	1.63E-06	1.51E-06	8.56	2.97E+03
MEAN	1.55E-06	1.43E-06	7.65	1.55E-06	1.43E-06	7.56	1773.96
S.D.	7.24E-08	6.77E-08	0.35	7.09E-08	6.79E-08	0.49	453.10
C.V.	4.67	4.74	4.62	4.57	4.73	6.54	25.54

Table 9: Results of the MS and P analyses of the soil sampled in Line 3 at Rizomilos 2 at two different depths (A & B). The abbreviations stand for: low frequency MS (χ_{lf}), high frequency MS (χ_{hf}), frequency dependent percentage (fd%) and parts per million (ppm). The table also shows the minimum (MIN) and maximum (MAX) values, as well as the mean, standard deviation (S.D.) and coefficient of variation (C.V.) of the measurements

PROFILE SAMPLES FROM LINE 3 (RIZOMILOS)											
Magnetic Susceptibility											
POINT A				POINT B				CONTROL			
Depth	χ_{lf}	χ_{hf}	FD (%)	DEPTH	χ_{lf}	χ_{hf}	FD (%)	DEPTH	χ_{lf}	χ_{hf}	FD (%)
0.20-0.25	1.59E-06	1.47E-06	7.74	0.20-0.25	1.49E-06	1.38E-06	7.95	0.19-0.25	9.77E-07	9.00E-07	7.88
0.25-0.30	1.57E-06	1.45E-06	7.81	0.25-0.30	1.57E-06	1.45E-06	7.09	0.24-0.32	1.01E-06	9.32E-07	7.90
0.30-0.37	1.50E-06	1.39E-06	7.03	0.33-0.43	1.51E-06	1.39E-06	7.80	0.31-0.36	9.23E-07	8.66E-07	6.10
0.37-0.47	1.46E-06	1.34E-06	7.86	0.43-0.52	1.45E-06	1.34E-06	7.82	0.36-0.42	9.34E-07	8.66E-07	7.23
0.47-0.56	1.33E-06	1.23E-06	7.65	0.52-0.57	1.34E-06	1.24E-06	7.45	0.42-0.47	9.07E-07	8.46E-07	6.64
0.56-0.65	1.24E-06	1.17E-06	6.02	0.57-0.68	1.26E-06	1.17E-06	7.29	0.47-0.54	9.14E-07	8.52E-07	6.81
0.65-0.75	1.27E-06	1.19E-06	5.65	0.68-0.76	1.17E-06	1.10E-06	6.23	0.50-0.20	9.73E-07	8.99E-07	7.62
0.75-0.84	1.26E-06	1.19E-06	5.86	0.76-0.85	1.07E-06	9.95E-07	6.86	0.54-0.60	8.99E-07	8.40E-07	6.55
0.84-0.93	1.26E-06	1.18E-06	6.82	0.85-0.94	9.16E-07	8.64E-07	5.68	0.60-0.62	8.79E-07	8.21E-07	6.70
0.93-1.04	1.27E-06	1.18E-06	6.59	0.94-1.03	6.41E-07	6.10E-07	4.81	0.62-0.68	8.79E-07	8.23E-07	6.38
				1.03-1.14	8.78E-07	8.32E-07	5.27	0.68-0.80	8.17E-07	7.69E-07	5.85
								0.80-0.88	8.26E-07	7.74E-07	6.23
								0.88-0.96	8.44E-07	7.94E-07	5.90
								0.96-1.02	8.43E-07	8.01E-07	5.02
MIN	1.24E-06	1.17E-06	5.65		6.41E-07	6.10E-07	4.81		8.17E-07	7.69E-07	5.02
MAX	1.59E-06	1.47E-06	7.86		1.57E-06	1.45E-06	7.95		1.01E-06	9.32E-07	7.90
MEAN	1.38E-06	1.28E-06	6.90		1.21E-06	1.12E-06	6.75		9.02E-07	8.42E-07	6.63
S.D.	1.41E-07	1.22E-07	0.85		3.0312E-07	2.72E-07	1.09		5.9059E-08	4.86E-08	0.82
C.V.	10.24	9.53	12.35		25.07	24.21	16.21		6.55	5.78	12.39

Table 10: Results of the MS analysis of the auger samples from Line 3 and the off-site controls collected at Rizomilos. The abbreviations stand for: low frequency MS (χ_{lf}), high frequency MS (χ_{hf}), frequency dependent percentage (fd%) and parts per million (ppm). The table also shows the minimum (MIN) and maximum (MAX) values, as well as the mean, standard deviation (S.D.) and coefficient of variation (C.V.) of the measurements.

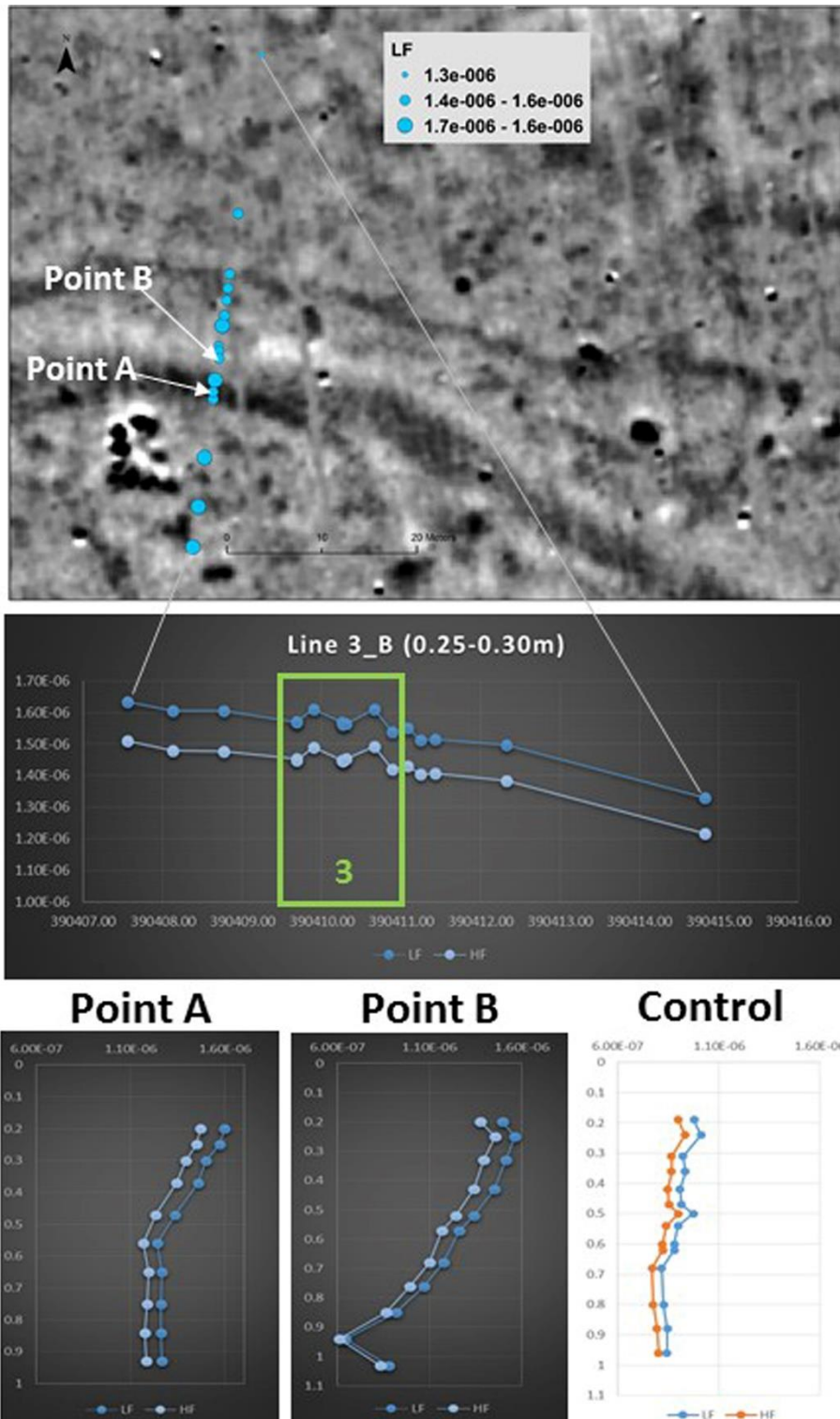


Figure 28: Bubble plot (above) and graph (middle) showing the lateral MS distribution along Line 3_B (Rizomilos). In the graph, the location of the targeted ditch-like positive magnetic anomaly is indicated in green (3). The location and results of the 'auger' samples are also shown (A, B & off-site Control).

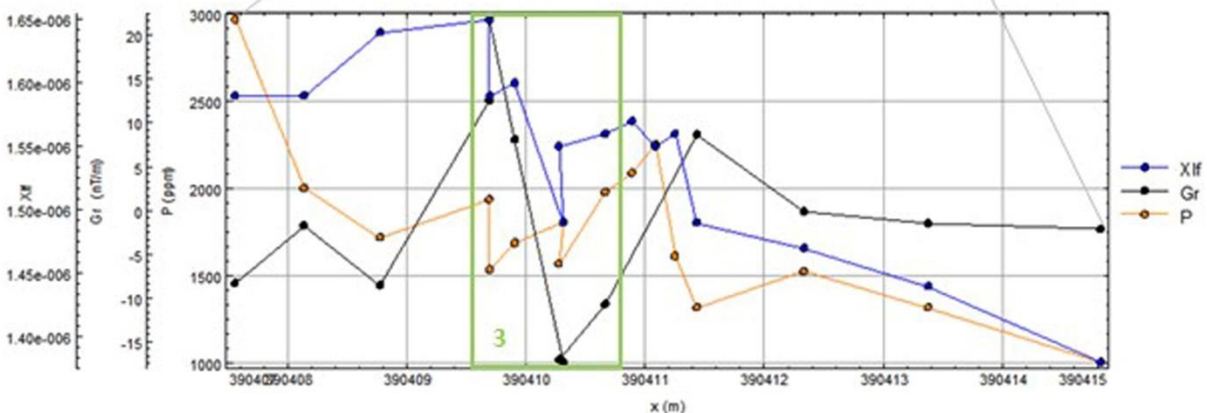
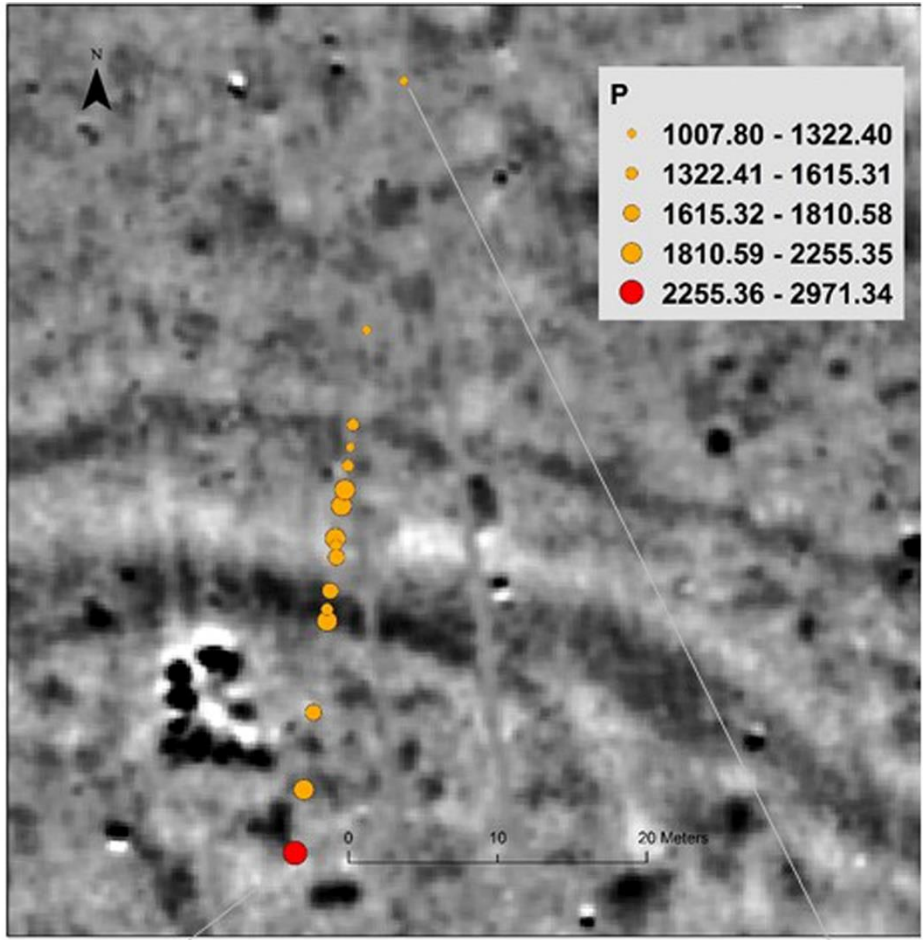


Figure 29: Bubble plot (above) showing the lateral P distribution along Line 3_B (Rizomilos). The bubble plot overlays the extract of the magnetometer data. The graph (below) shows the lateral variation of the magnetic intensity (Gr) and the MS (X_{if}) and P. In the graph, the location of the targeted ditch-like positive magnetic anomaly is indicated in green (3).

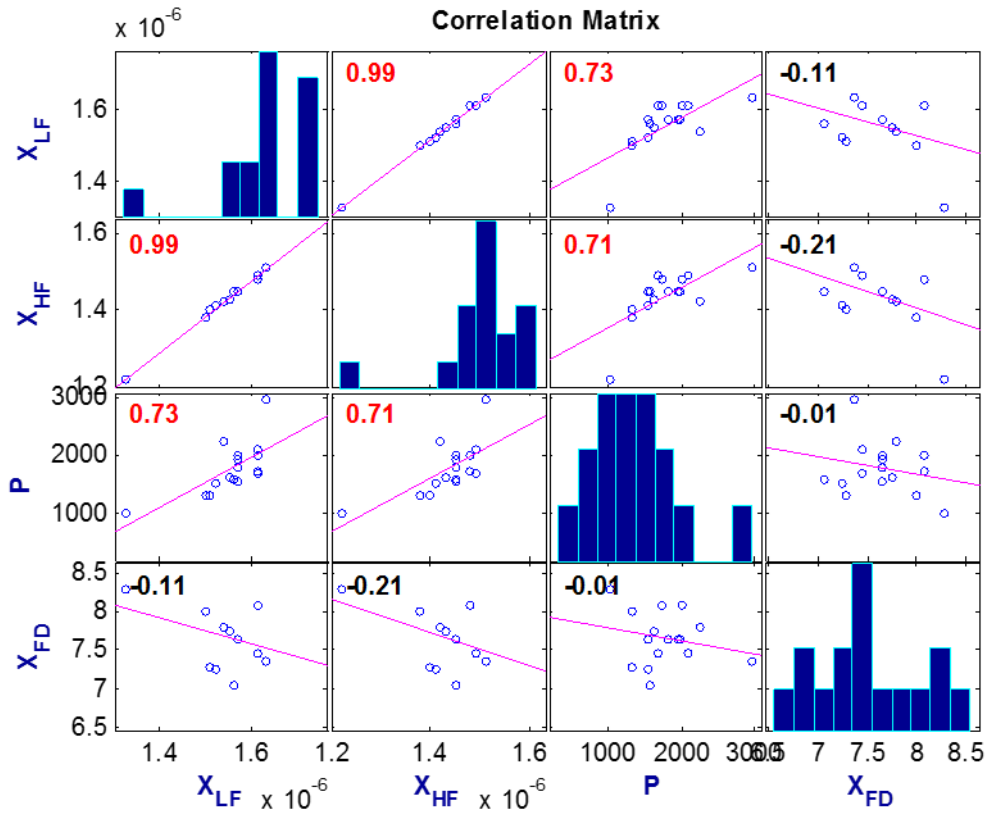


Figure 30: Results of the Spearman correlation (Line3_B, Rizomilos 2)

Integration of Results

The geophysical investigations at magoula Rizomilos2 were carried out through the employment of magnetic (SENSYS), soil conductivity/magnetic susceptibility (EM GEM2 and CMD) and GPR (Noggin Plus 250MHz and MALA MIRA 400MHz) techniques. The largest coverage of the site was accomplished through the magnetic survey that covered more than 106,000 square meters. The east and north sections of the site were covered through EM techniques and small patches to the east and south were covered via GPR techniques, even though measurements from both units were not that effective in this survey.

The circular shape of the magoula is also evident from the topographic map, reaching a relative altitude of about 8m with respect to the surrounding flat areas. At the center of the site (close to the top of the elevation), a large illegal farmstead has been installed. The fields on the magoula and the surrounding area were cultivated by corn, alfalfa and cotton. It became evident that the plowing activities have disturbed the cultural layers of the site, but still it was possible to recognize a wealth of subsurface anomalies. According to the vertical electric soundings, the plow zone (with resistivity of 62 Ohm-m) covers the first 0.6m and the cultural layers (resistivity of 25 Ohm-m) extend below it up to a depth of about 2.2m.

Magnetic data have shown that the main locus of the magoula extends over an almost circular area of diameter spanning from 210-250m. To the east of it, another smaller locus of magnetic anomalies has been identified, in accordance to the satellite images, suggesting a neighboring settlement extending in the particular location. The main magoula of Rizomilos 2 is confined by a series of 2-3 concentric ditches (A1, A2 and A3) of width 3-5m. These features were also confirmed by the GEM-HCP magnetic susceptibility measurements for a depth range of 0-1.7m. Within the specific ditches, another series of enclosures (B1, B2, B3 and B4) appears, having a much smaller width (<2m) and a magnetic signature very different to the one of the wider ditches, suggesting the existence of fortifications. The ditches seem to be relatively well preserved with the exception to the north direction. Four main gates to the settlement are suggested by both the openings to the ditches and to the fortification walls: G1 and G4 are located at opposite sides along the E-W directions, while G2 and G3 are located at opposite sides along the NW-SE directions. Another system of gates may exist along the S-N directions according to the breaks that are formed by the fortification walls, but which are not obvious to the ditches to the south.

Magnetic data have also indicated a number of candidate structural remains. Only two of them (C3 and C4) are located in the core habitation zone of the magoula. The rest of the structures seem to be located in the periphery of it, with C1, C10, C14 and the cluster of C7, C8 and C9 located close to the gates of the magoula. Almost all of them are longhouses and a few (C4, C6, C7 and C8) seem to consist of two rooms. The structural anomalies seem to be more in accordance with the outer and wider enclosures, rather than with the inner and thinner enclosures. This supports the case that the enclosures may belong to different phases of occupation.

Moving towards the east, the magnetic measurements indicated another suspicious series of enclosures (B5 and B6) looking like fortification walls encircling a small area than the main magoula. The concentric pattern of these rings may suggest another smaller settlement, which

may have pre-existed the main magoula, as it is close to the flooding susceptibility zone of the region. Indeed, the suspected settlement is located on a smoother elevation of the terrain and the flooding simulation indicated that a 1m rising of the water level goes all around the particular zone, following the curvature of the enclosures. This is also compatible to the rest of the ditches (A5, A6, A7, A8 and A9) that are revealed to the north. The main feature, A6, was also confirmed by the EM conductivity measurements, located at deeper strata and may be correlated to a paleochannel instead of a ditch. Similarly, a 1.5m rise of the water table could have reached the outer ditch of the main magoula. It has to be mentioned that based on the oral testimonies of the villagers, even in historical times, the area was repeatedly flooded, which is also expected due to the vicinity of the magoula to Lake Karla.

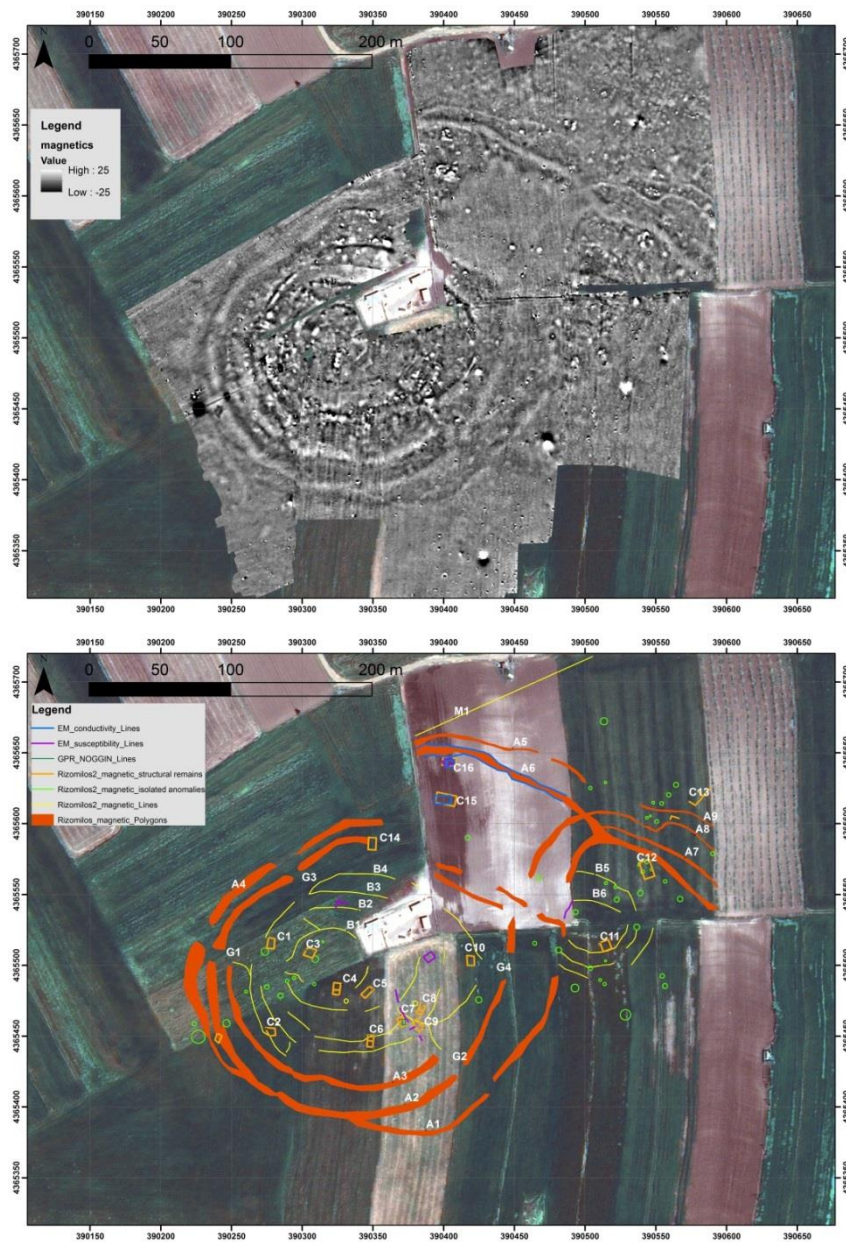


Figure 31: Interpretation of magnetic results

Only one small structure (C11) was indicated by the magnetic data within the nucleus of the second magoula and one more (C12) existing at its periphery to the north, outside the fortification walls and close to the paleochannel A6. Two more structures (C15 and C16) were identified by both magnetic and EM surveys to the north of the main magoula and close to the paleochannel A6. The above indicate that despite the weak clustering of habitation within the main magoula of Rizomilos 2, there was probably a more dispersed habitation outside the limits of the magoula. It may be also possible that the second magoula was an earlier settlement.

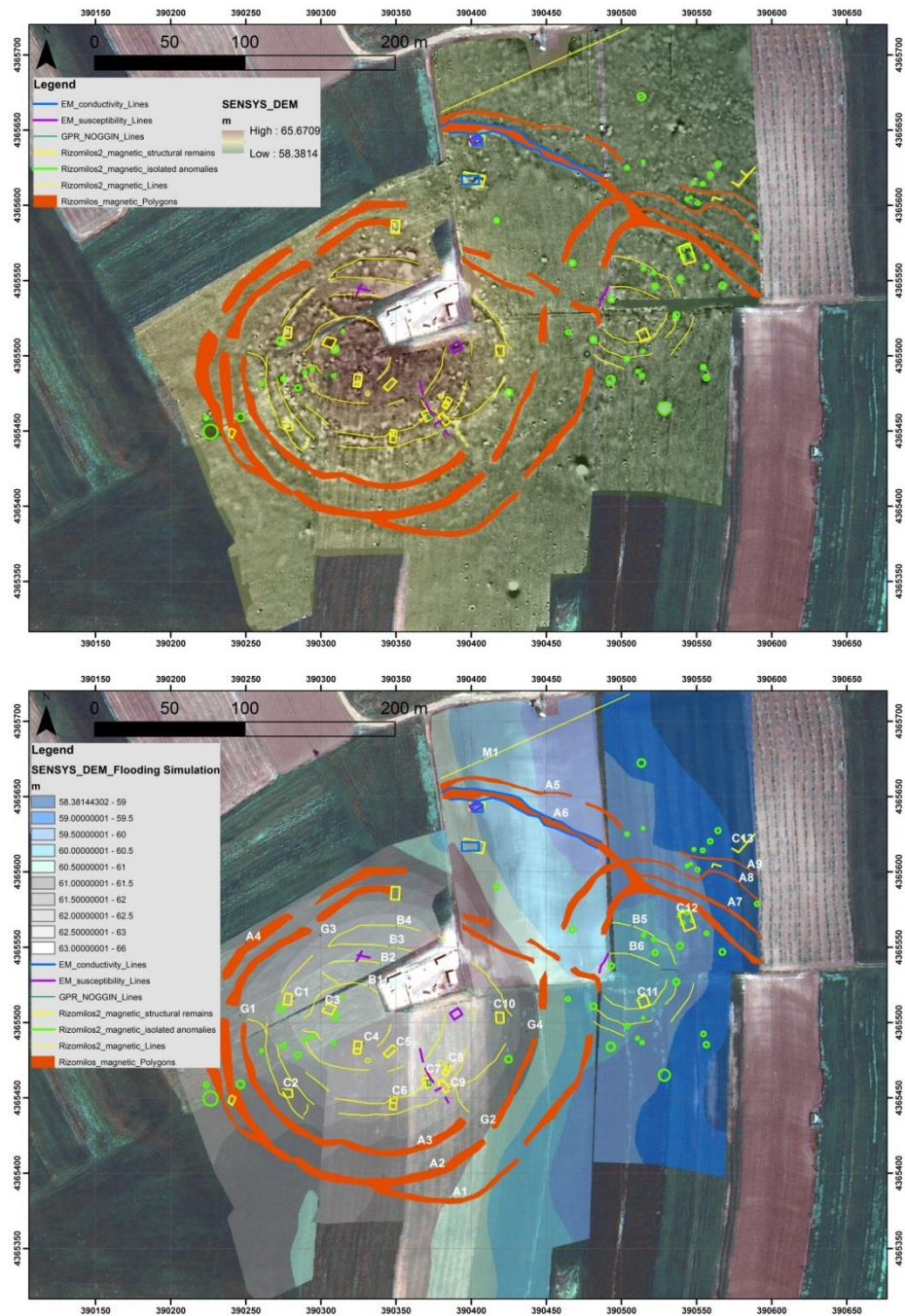


Figure 32: Results of prospection overlaid with flooding simulation

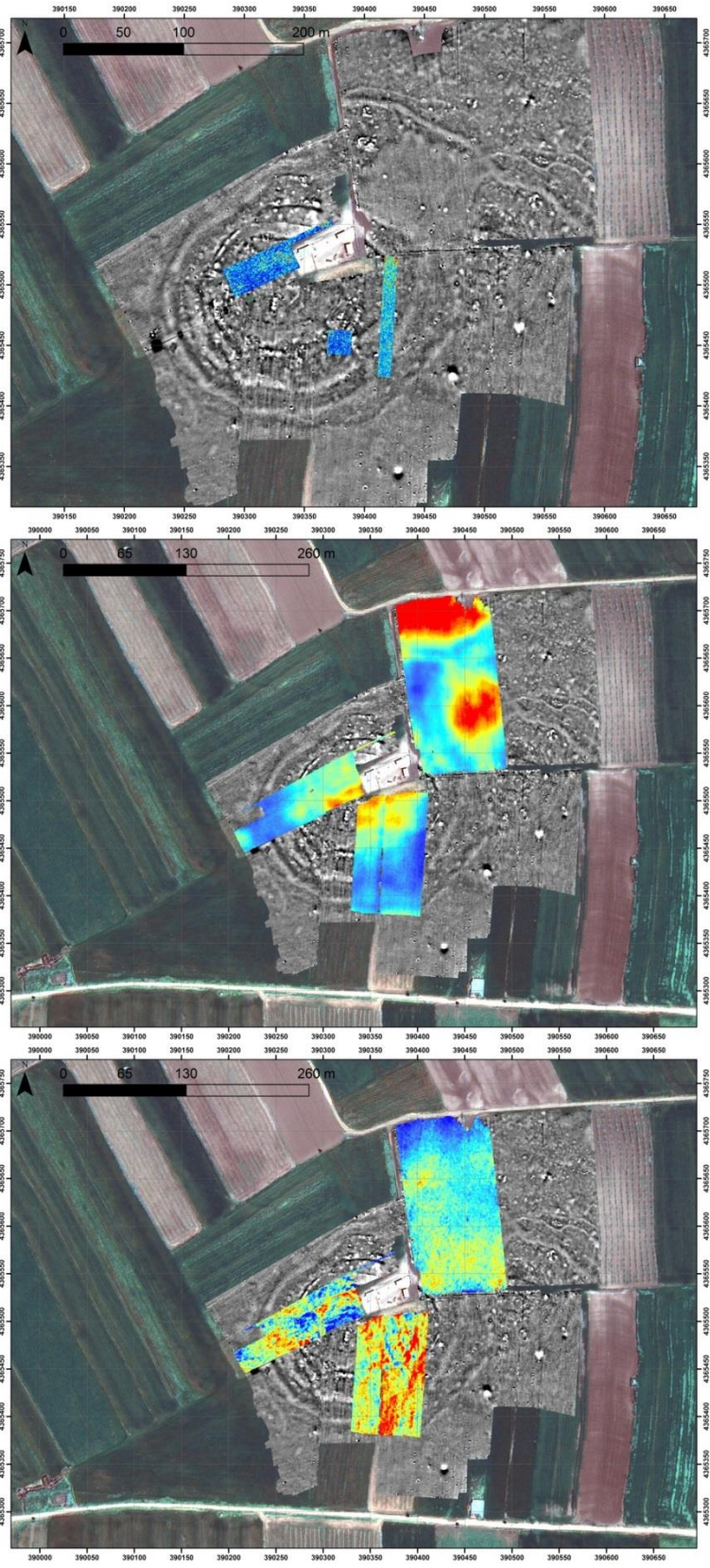


Figure 33: The comparison of different prospection methodologies in Rizomilos 2

In regards to soils studies, the lines collected across the concentric ditch-like magnetic anomalies defining the main magoula at Rizomilos (Line 1 & 2 in Figure 14) showed an unexpected decreasing MS distribution from the outside towards the center of the site. This reverse pattern could be a consequence of the truncation of putative archaeological layers/structures by agricultural practices and especially at the center of the site. Actually, there is a large illegal farmstead close to the top of the magoula (blank area near to the top of the elevation in Figure 15). Therefore, it is possible that modern leveling and other infrastructure works related to the farm have heavily disturbed this area of the site.

In the case of the P analysis, all the lines showed the expected P enhanced values in the samples collected towards the center of the magoula. The highest P values were obtained from (Line 1 and 2), in the area immediately inside the innermost concentric ditches defining the main magoula (2 in Figure 17 and 1 in Figure 20). In this area, a series of narrower (<2m) and concentric anomalies of stronger magnetic intensity were also detected and interpreted as enclosures. The P enhancement in the spaces within these possible enclosures seems to indicate the core of the anthropogenic activity (potential husbandry activity?).

The concentric ditch-like anomalies were characterized by enhanced MS values. The highest MS values ($1.82E-06$) were measured in the innermost concentric ditch at the north of the survey area (point B in Line 2, Figure 19). The FD results obtained from these samples (Table 8) were also fairly high (mean=8.07%) with the highest value (8.37%) at 0.60-0.69m depth. The MS enhancement correlated with high gradients in the magnetic datasets (Figure 20). Whilst the P analysis was not carried out with the auger samples, the P results obtained from the lines did not reveal particular P enhancements in the samples collected at the locations of the concentric ditches. Therefore, these ditches seem not to have been a focus of accumulation of organic matter (as expected from the disposal of refuse material from the anthropogenic activities within the magoula).

The only clear MS increasing pattern towards the 'center' of the magoula was obtained from Line 3 (Figure 14). The results of the P analysis followed the same pattern. This line was crossing the outermost linear ditch-like anomaly (3 in Figure 22 and 23), instead of concentric ditches mentioned above. The line did not reach the actual center of the main magoula but reached other positive magnetic anomalies that have been interpreted as possible structures. Therefore, the MS and P enhancement could be related to these potential areas of habitation to the south of the targeted linear ditch-like anomaly.

Whilst the linear ditch targeted with Line 3 was also characterized by enhanced MS values, these were lower than those obtained from the concentric ditches (χ_{lf} mean= $1.28E-06$ m^3kg^{-1} , Table 10). The FD results were also significantly lower (mean=6.90%). These lower MS values could define a different type of ditch-like feature (e.g. paleochannel?) in comparison with the concentric ditches (e.g. opened to collect clay to build structures in the center of the magoula and re-used for the refusal of burnt and possibly non-organic material). However, this lower MS could be also indicating a shallower or highly truncated feature. This later hypothesis supports an interpretation of the magnetic and EMI data which suggests that the particular feature represents a halo left from a past flooding episode. Further characterization of the auger samples taken inside this and the concentric ditches could clarify the nature of such features. In any case, it seems that all of these ditch-like features were bottomed at least at ~1m depth.

Site Bibliography

Grundmann K., 1937. *Magula Hadzimisiotiki*, AM 62, 56-69., 37, taf. 37A

Halstead P., 1984. *Strategies of survival: an ecological approach to social and economic change in the early farming communities of Thessaly, N. Greece*, Cambridge, (PhD Thesis), 237 (no 157)

Αποστολοπούλου - Κακαβογιάννη Ο., 1986. Τοπογραφία της περιοχής των Φερών Θεσσαλίας κατά την προϊστορική περίοδο, *ΑΔ* 34 (1979), 174-206.

Αρβανιτόπουλος Α.Σ., 1910. *Αι εν Χαιρωνεία και κατά την Φωκίδα Ανασκαφαί*, ΠΑΕ (1909), 123-171.

Βουζαξάκης Κ., 2009. *Νεολιθικές θέσεις στη Μαγνησία. Ανασκόπηση – Ανασύνθεση δεδομένων*, στο Αρχαιολογικό Έργο Θεσσαλίας και Στερεάς Ελλάδας 2 (2006), τ. Ι, σελ. 61-74.

Γαλλής Κ., 1992. *Ατλας Προϊστορικών Οικισμών της Ανατολικής Θεσσαλικής Πεδιάδας*, Λάρισα, 176 (ΑΤΑΕ 282)

Θεοχάρης Δ.Ρ., 1973. *Νεολιθική Ελλάς*, Αθήνα. χάρτης 4, αρ. 94